



Università Politecnica delle Marche
Scuola di Dottorato di Ricerca in Scienze dell'Ingegneria
Curriculum in Ingegneria Civile, Ambientale, Edile e Architettura

A novel failure model to predict biofouling (algae growth) on different building facades under different environmental conditions

Ph.D. Dissertation of:
Andrea Gianangeli

Advisor:

Prof. Marco D'Orazio

Coadvisor:

Prof. Enrico Quagliarini

Curriculum supervisor:

Prof. Stefano Lenci

XVII edition - new series



Università Politecnica delle Marche
Scuola di Dottorato di Ricerca in Scienze dell'Ingegneria
Curriculum in Ingegneria Civile, Ambientale, Edile e Architettura

A novel failure model to predict biofouling (algae growth) on different building facades under different environmental conditions

Ph.D. Dissertation of:

Andrea Gianangeli

Advisor:

Prof. Marco D'Orazio

Coadvisor:

Prof. Enrico Quagliarini

Curriculum supervisor:

Prof. Stefano Lenci

XVII edition - new series

Università Politecnica delle Marche
Dipartimento di Ingegneria Civile, Edile e Architettura (DICEA)
Via Brezze Bianche — 60131 - Ancona, Italy

alla mia famiglia

Acknowledgments

The multidisciplinary topic of this research implicated the cooperation of several experts in different fields but, first of all, I must thank my supervisor, Prof. Marco D’Orazio. Thank you, not only for sharing to me your expertise and the scientific guidance, but also for the chances and to believe in me. Thanks for all your help, time and patience!

My gratitude then goes out to Prof. Enrico Quagliarini, who, by also supervising me, gave a significant contribution, always being open to discussion with his critical look as “outsider”. I would also like to thank Prof. Elisa di Giuseppe for her advices and comments concerning my works as well as her encouragement during my PhD course. Thank you for all suggestions, reservations, explanations and honest opinions during these three years. I am very grateful to you.

Of course, I want to thank Lorenzo Graziani, who introduced me in this research. I wish also to acknowledge Prof. Andrea Osimani and Prof. Lucia Aquilanti for their assistance and the many practical information and good advice in the field of biological growth.

I have spent many hours in the laboratory, and a special word of thanks is owed to Giuliano Giuliani and Daniele Mannocchi, for the practical support in my experiments during the first year.

I would also like to thank all my colleagues of DICEA, for making my daily life a really pleasure. A special thanks to Benedetta, for her help in completing my research. Thank you for all the support!

Last but not least, I would like to thank my family, and above all Veronica, who helped me carrying the load of setbacks, consistently and patiently encouraging me with their understanding and active help. Thanks a lot!

Ancona, November 2018

Andrea Gianangeli



This project has received funding from the European Union’s Horizon 2020 research and innovation programme under grant agreement No 637268.

Abstract

The building envelopes are often exposed to algal biofouling, that causes the deterioration of the materials' surface, with consequence in economic loss due to the building maintenance. Biofouling on façades is firstly due to the algal colonization, mainly promoted by green algae and cyanobacteria, that also can favour the proliferation of other microorganisms (i.e. moulds, lichens). Only few studies tried to investigate the suitable conditions for algae to grow on construction materials, hence a failure model has not been implemented yet.

This research tried to fill this gap by presenting a mathematical model able to predict algae growth on building materials exposed to the environmental conditions and considering the substrate properties. The failure model was based on experimental results and on the Avrami's law.

Algae biofouling was investigated on fired brick substrates, through accelerated growth tests under different environmental conditions of temperature and relative humidity. It was found that temperature mainly influenced the algae growth rate (covered area as a function of time), while at relative humidity lower than 98% no growth activity was detected. Regarding the effect of the substrate, roughness and high porosity favoured the colonization in terms of velocity of the growth process.

The quantification of algae biofouling was based on the covered area measured during the experiments. The model consists of several equations describing the growth rate by algae on the substrates under different environmental conditions, including the effect of exposure time, temperature, relative humidity. The parameters and the numerical values included in the model were fitted for bricks and stones, but the model can be valid also for other building materials. Moreover, if implemented into a simulation software, the biofouling process on façades could be predicted, and it could help in providing guidelines for intervention and maintenance techniques in specific context.

Contents

| | | |
|-------|---|----|
| 1 | Introduction..... | 1 |
| 2 | Biofouling on building façades | 3 |
| 2.1 | Impact of internal insulation on hygrothermal behaviour of the wall | 3 |
| 2.2 | Biodeterioration of the building envelope caused by algae colonization | 4 |
| 2.3 | Microalgae and Cyanobacteria..... | 5 |
| 2.4 | Essential factors for algae growth | 5 |
| 3 | Theory and equations | 7 |
| 3.1 | Avrami's theory and the existing predictive model | 7 |
| 3.2 | New failure model based on the Avrami's law | 9 |
| 4 | Experimental program..... | 13 |
| 4.1 | Algae cultures | 15 |
| 4.2 | Tested building materials | 16 |
| 4.3 | Preliminary tests about the influence of temperature on algae growth | 18 |
| 4.4 | Accelerated growth tests under different constant relative humidities..... | 19 |
| 4.5 | Accelerated growth tests under different temperatures | 20 |
| 4.6 | Measurement and evaluation of algae growth..... | 21 |
| 5 | Calculation methodology | 25 |
| 5.1 | Experimental determination of Avrami's parameters and scale functions | 25 |
| 5.1.1 | Experimental Avrami's parameters | 25 |
| 5.1.2 | Experimental scale functions for the effect of environmental conditions .. | 25 |
| 5.2 | Analytical determination of Avrami's parameters and scale functions | 26 |
| 5.2.1 | Domains and codomains | 26 |
| 5.2.2 | Data fitting for the determination of the failure model equations | 27 |
| 5.3 | Validation of the new failure model..... | 27 |
| 6 | Experimental results..... | 29 |
| 6.1 | Results of preliminary algae growth tests under different temperatures | 29 |
| 6.2 | Results of accelerated growth tests under different constant relative humidities..... | 31 |
| 6.3 | Results of accelerated growth tests under different constant temperatures | 35 |

| | | |
|-----|---|----|
| 6.4 | The influence of substrate properties on algae growth under constant temperatures..... | 41 |
| 7 | Modelling of the experimental results..... | 45 |
| 7.1 | Effect of temperature modelled with the previous Avrami's model | 45 |
| 7.2 | Results about the scaling effect of environmental conditions | 48 |
| 7.3 | Equations of the implemented Avrami's parameters based on fired bricks | 49 |
| 7.4 | Equations of the scale functions of environmental conditions based on fired bricks..... | 52 |
| 7.5 | Corrective coefficients for stone materials..... | 55 |
| 7.6 | Validation of the failure model | 56 |
| 8 | Conclusions..... | 63 |

List of figures

| | |
|---|----|
| Figure 2.1. a) Discolouring effect of biological growth on a historical façade; b) Growth of green algae on a wall [42]. | 4 |
| Figure 3.1. Typical growth of a micro-algae culture. | 7 |
| Figure 3.2. A qualitative example of the implemented failure model: a) determination of the growth curve under each exposure condition; b) the overall process of covered area by algae biofouling under variable environmental conditions over the time. | 12 |
| Figure 4.1. a) Assembled measurement system with SHT31-D sensors and NI myRIO-1900 data logger; b) Protected T/RH sensor positioned near the samples inside a growth chamber during the accelerated tests. | 14 |
| Figure 4.2. Mixed microalgae suspension of <i>Chlorella mirabilis</i> and <i>Chroococcidiopsis fissurarum</i> after incubation. | 16 |
| Figure 4.3. a) Brick samples prepared for the experimental investigations;b) Mercury intrusion porosimetry for the characterization of the sample substrates. | 17 |
| Figure 4.4. Magnification of a brick surface (sample B-2R) by the optical profiler for roughness determination. | 18 |
| Figure 4.5. a) Algae cultures were incubated in controlled environment under different constant temperatures; b) Counting of the number of cells of the tested cultures in a Thoma-Zeiss hemocytometer under a light microscope. | 19 |
| Figure 4.6. a) View of the glass chambers used to maintain different constant relative humidities; b) Scheme of the test apparatus build up for investigations on relative humidity effect. | 20 |
| Figure 4.7. a) View of the inside growth chamber used for the evaluation of temperature influence on algae biofouling; b) Scheme of the run-off test apparatus built up for the accelerated tests. | 21 |
| Figure 4.8. a) Colorimetric measurements on the same points of the samples' surface during the test; b) Digitalization of the samples' surfaces for the biofouling extent evaluation. | 22 |
| Figure 4.9. An example of binarization process; from left to right: scanned images from the original sample were elaborated by a filtering process (threshold method) to obtain binary images. | 23 |
| Figure 6.1. Growth curves of: a) <i>Chlorella mirabilis</i> CM; b) <i>Chroococcidiopsis fissurarum</i> CF; c) mixed culture MIX. The growth of the microbial species was tested at five different temperatures. | 30 |
| Figure 6.2. Total colour difference ΔE : a) RH ₁ =75%; b) RH ₂ =87%; c) RH ₃ =98%. | 32 |
| Figure 6.3. Red/green colour difference Δa of sample B-5R_98. | 33 |

| | |
|--|----|
| Figure 6.4. Evolution of the brick samples' surface tested under three different RHs from the beginning (t=0 week) to the end of the test (t=36 weeks)..... | 34 |
| Figure 6.5. Progressive algae coverage on B-2 samples' surfaces during accelerated growth test under different constant temperatures. | 36 |
| Figure 6.6. Progressive algae coverage on B-3 samples' surfaces during accelerated growth test under different constant temperatures..... | 37 |
| Figure 6.7. Progressive algae coverage on B-5 samples' surfaces during accelerated growth test under different constant temperatures..... | 38 |
| Figure 6.8. Average area coverage area of fired bricks: a) samples B-2R; b) samples B-2S; c) samples B-3; d) samples B-5R; e) samples B-5S. Results for T=10°C are displayed in black, while results for T=27.5 °C in grey. Vertical lines indicate standard deviations. | 40 |
| Figure 6.9. a) Duration of the accelerated biofouling process on tested fired bricks in ascending order of porosity; b) Average covered area by algae at the end of the tests on tested bricks in ascending order of roughness; c) Time needed for a complete biofouling process on samples in ascending order of total pore area; d) Final average covered area on samples in ascending order of total pore area. | 42 |
| Figure 6.10. SEM micrographs (magnification 500x) of B-2R and B-5R samples collected at the end of the accelerated growth test. a) On B-2R sample, algae and cyanobacteria (green arrow) grown close to the pores, taking advantage of the micro-asperities of the substrate but leaving free the smoother surface (red arrow); b) On B-5R sample, algae and cyanobacteria grown inside pore cavities (green arrows) and adhered to the many irregularities of the surface.. | 43 |
| Figure 7.1. Overlapping of the Avrami's curves to experimental data: a) B-2R and AS samples; b) B-3 sample; c) B-5R and B-5S sample. Results for T=10°C are reported in black, results for T=27.5°C are reported in grey, red dotted lines indicate Avrami's curves. Vertical lines indicate standard deviations. | 46 |
| Figure 7.2. Correlation between experimental and calculated Avrami's parameters for fired brick materials: a) final covered area ratio A_c/A_t , b) growth rate K , and c) latency time t_l | 51 |
| Figure 7.3. Trend of the scale functions a) τ_A and b) τ_K for the tested fired brick materials. | 54 |
| Figure 7.4. Growth curves, calculated with the implemented failure model, on the fired brick materials tested in this research under optimal environmental conditions (Test_0). Vertical lines indicate the standard errors of experimental measurements. | 57 |
| Figure 7.5. Growth curves, calculated with the implemented failure model, on the fired brick materials tested in Graziani et al. [21] under optimal environmental conditions (Test_0). Vertical lines indicate the standard errors of experimental measurements. | 58 |

| | |
|---|----|
| Figure 7.6. Growth curves, calculated with the implemented failure model, on the fired brick materials tested in this research under cold temperature (Test_5). Vertical lines indicate the standard errors of experimental measurements..... | 59 |
| Figure 7.7. Growth curves, calculated with the implemented failure model, on the stone materials: a) sandstones and b) limestones; tested under optimal environmental conditions (Test_0). Vertical line bars indicate experimental standard deviations. | 60 |
| Figure 7.8. R factor values for a) fired brick materials and b) stone materials. Dotted lines indicate the limit of an acceptable R factor. | 61 |

List of tables

| | |
|---|----|
| Table 4.1. Environmental conditions during the accelerated growth tests on building materials. | 13 |
| Table 4.2. SHT31D sensor performance specifications..... | 14 |
| Table 4.3. Composition of the stock solutions used for the preparation of the BBM (Bold Basal Medium). | 15 |
| Table 4.4. Substrate properties of tested fired brick materials (mean value \pm standard deviation). In brackets references of previous works are reported. | 16 |
| Table 4.5. Substrate properties of tested stone material (mean value \pm standard deviation). In brackets references of previous works are reported. | 17 |
| Table 7.1. Avrami's parameters determined after the accelerated tests at constant temperature on fired bricks..... | 47 |
| Table 7.2. Ω values determined from experimental results under tested relative humidities. | 48 |
| Table 7.3. Experimental results for τ_A and τ_K of Test_5 (T=10 °C). | 48 |
| Table 7.4. Avrami's parameters for fired brick materials: regression coefficients associated to the substrate variables (porosity P , roughness R and total pore area A). | 49 |
| Table 7.5. Regression coefficients determined for the substrate variables (P , R , A) of the temperature scale functions τ_A and τ_K | 53 |
| Table 7.6. Calculated values of corrective coefficients for sandstone and limestone materials. | 55 |

Nomenclature

| | |
|-----------------------|---|
| L_0^*, a_0^*, b_0^* | colour coordinates of samples before the beginning of the test [-] |
| L^*, a^*, b^* | colour coordinates of samples during the test [-] |
| ΔE | total colour variation [-] |
| Δa | red/green colour variation [-] |
| X | covered area [-] |
| t | time [day] |
| Λ | Avrami's constant [-] |
| n | Avrami's exponent [-] |
| γ | number of algal spots at time t per unit area [-] |
| k_c | growth rate constant [$\mu\text{m}/\text{day}$] |
| k_g | specific attachment constant [$\text{spot}/\mu\text{m}^2 \text{day}^2$] |
| $d\gamma/dt$ | specific attachment rate [$\text{spot}/\mu\text{m}^2 \text{day}$] |
| S | surface of an algal spot [μm^2] |
| P | total porosity [%] |
| R | roughness [μm] |
| A | total pore area [m^2/g] |
| T | temperature [$^{\circ}\text{C}$] |
| RH | relative humidity [%] |
| A_c/A_t | parameter of final covered area ratio [-] |
| K | parameter of growth rate [-] |
| t_l | parameter of latency time [day] |
| τ_{Λ} | scale function of temperature on A_c/A_t [-] |
| τ_K | scale function of temperature on K [-] |
| Ω | scale function of relative humidity [-] |
| a, \dots, v | regression coefficients [-] |
| α, \dots, μ | corrective coefficients [-] |

Chapter 1

Introduction

This PhD research is a part of the European research project *RIBuild* (Robust Internal Thermal Insulation of Historic Buildings) [1]. The aim of *RIBuild* is to develop effective and comprehensive guidelines on the implementation of internal thermal insulation in historic buildings, in order to reduce the energy consumptions without compromising the building heritage. The thermal upgrade of historic facades is a crucial aspect, as the insulation options are generally limited to the internal insulation, because of the constructive features and aesthetical worth preservation [2–5].

However, the retrofit of external walls changes the hygrothermal performance of the wall itself, and it can lead to damages, or in the worst case to the building failure [6,7]. It is important to investigate how and under what conditions the internal thermal insulation can be applied with an acceptable safety level against failure and without degrading the building structures. The idea is to maximise energy savings without involving collateral damages related to e.g. freeze-thaw, mould growth or dry rot [2,6,8–10].

Each type of building has specific characteristics that need to be addressed during renovation and therefore several factors should be considered. Among these, some of the most important factors are not only the properties of the building materials and their threshold values for failure when adding internal insulation, but also the climatic conditions to which the building is exposed.

The issue deepened in this PhD thesis mainly focused in the work package WP2 (“Material characterisation coupled with eligible renovation measures”) of *RIBuild* project, and in particular in Task 2.3 (“Limit and threshold for failure”). The main objective of WP2 is to provide data about building material properties and threshold values for historic building materials as a background for material characterisation models. Failure in the construction, associated to the overcome of a limit state, often occurs as a result of the hygrothermal conditions altered after the implementation of an internal insulation. Failure is for instance expressed as freeze-thaw damage of stone and brick used for the external wall [9], or mould growth [11–13], or rot in wooden parts of a suspended floor that rest on the inner part of the external wall [6–8]. Moreover, in literature can be found several studies that proposed numerical modelling of the microbial growth aimed to predict the biofouling on building components [11–17].

Failure models about mould growth were highly investigated and developed [13,15,16], while they are very limited about algae growth. In fact, only few studies have attempted to model the biofouling on external side of the building envelope [18–22]. Moreover they are mainly related to the Avrami’s model at fixed optimal temperatures for the biological growth [19–22]. Thus, further researches are needed to investigate the effects of different environmental conditions, characterized also by non-optimal temperatures and different level of relative humidities. Furthermore, up to now the “modified” Avrami’s model [19,22] does

not give the possibility to directly introduce the influencing factors related to the substrate and the environmental conditions as input variables in the calculation. Hence, in order to become a real failure model useful to predict the algae growth on building materials and the consequent biodeterioration of façades, the Avrami's model needs to be implemented.

In this way, the aim of this research is to directly make explicit the main influencing factors of the substrate and of the environmental conditions into the “modified” Avrami's model, so as to have a real failure model able to predict algal biofouling on different building materials substrate and under variable environmental conditions. Therefore, researchers and practitioners will be able to make quantitative predictions which may help to provide guidelines for intervention and maintenance techniques [23–25].

Chapter 2

Biofouling on building façades

2.1 Impact of internal insulation on hygrothermal behaviour of the wall

To reduce the energy consumption of the existing stock building and improve the thermal performance of the building, an exterior thermal insulation system is generally considered as a good solution. However, even if it could be the best option in term of thermal performance, sometimes the exterior insulation is not possible due to architectural, esthetical and economic reasons. On the contrary, internal thermal insulation is often the only applicable technique to retrofit the existing walls, especially for historical buildings [2–5].

However, this insulation intervention needs to be executed with care: some authors showed how the installation of an internal insulation, especially in masonry walls, could lead to a variation of hygro-metric loads and moisture contents [6,7,26]. The hygrothermal conditions in the original wall could become worse in case of the application of a thermal insulation to the interior side, since, the heat flow coming from the room to the original wall is strongly reduced [4]. This new configuration can originate the possibility of condensation behind the insulation panels [2,27,28]. The moisture content inside the original wall could increase, leading to high moisture content on the cold side of the newly added insulation materials [2,5,28–31].

Therefore, the original masonry remains at the colder side of the wall, and this leads to a reduction of the drying potential towards the room. In fact, the implementation of an interior insulation system can act as a barrier, which oblige the water inside the masonry to migrate only towards the external side, increasing the unwanted moisture accumulation in that layer [8,29,32,33]. Thus, the consequences are not only inside the masonry, for instance causing a possible decay of embedded wooden beams [6,8,34], but also on the external side of the wall, by increasing the risk of frost damage [9,35] and biological growth [2,10,36].

Considering that the more porous a material is, the more moisture it can contain, the historic masonry walls, that are generally built by porous bricks and natural stones without plaster, are greatly exposed to moisture impact [32,37,38]. To avoid or at least reduce the moisture and the above mentioned related problems, vapour diffusion barriers have been recommended to disable vapour diffusion from the inside to outside, as well as capillary active porous insulation materials [39,40] and hydrophilic insulation materials can be used [41].

2.2 Biodeterioration of the building envelope caused by algae colonization

In addition to the possible consequence of the internal insulation on the increased moisture content on building façades after an internal insulation retrofit, it should be taken into account that the building envelope is also continuously exposed to open air and to weather conditions. For this reason façades are inevitably subjected also to the deterioration due to natural causes [42,43]. This process can start and also be accelerated by the presence microorganisms, which is a potential threat to the preservation of the building envelope. Both historic and modern materials on external walls are subject to the deteriorative and degradative action of the environment and living microorganisms (Figure 2.1a) [44].

Damages, deriving from metabolic activity of microorganisms, are mainly related with physical, chemical and aesthetical mechanisms [45]. It has been reported that the presence of a microbial layer may facilitate the production of acids and the biochemical deterioration of the material through the etching of mineral components and dissolution of binding minerals, especially in carbonates. Biophysical deterioration of the materials may also occur. Considerable force may be exerted through repeated shrinking and relaxing of the slimy sheath of the cyanobacteria during their cycle of drying and moistening. This eventually loosens mineral grains of the stone surface [45,46].

Another effect of the presence of biofilm on exposed surfaces, is the acceleration of the accumulation of atmospheric pollutants. The slimy surfaces of these microorganism facilitate adherence of airborne particles of dust, pollen, oil, and coal ash, giving rise to hard crusts and patinas that are difficult to eliminate [45]. On the other hand, the intensity of damages is highly correlated with: type and dimension of the microorganism involved; kind of material and state of its conservation; environmental conditions and micro-climatic exposure; level and types of air pollutants [45].

The living species dwelling on these materials are ranging from microscopical bacterial cells to higher plants and animals [45]. The main colonizers of building façades are algae and cyanobacteria [47,48], since they can live on a great variety of substrates. However, algal biofouling could also become a suitable habitat for further different species, like mould and fungi (Figure 2.1b) [42].

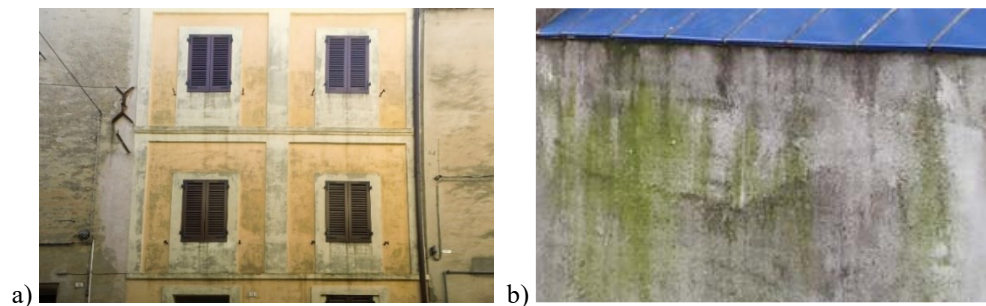


Figure 2.1. a) Discolouring effect of biological growth on a historical façade; b) Growth of green algae on a wall [42].

Loss of aesthetic value is considered one of the most obvious type of damage caused by algae. Algal communities are usually readily recognizable on building exposed surfaces because they form patina or sheets varying in extent, thickness, consistency, and colour. In well-lit and relatively dry environments, patinas are thin, tough, sometimes green, and very often grey or black, depending on the different-coloured pigments of the algae [46,49,50].

2.3 Microalgae and Cyanobacteria

Algae are one of the ancient living microorganisms. They are unicellular and pluricellular microorganisms, which can be divided into two groups: green algae (eukaryotic) and Cyanobacteria (prokaryotic). Some algae, named terrestrial algae, can live in terrestrial environments, for instance in soil or on tree trunks, and also on building façades [42–44,50–54].

Terrestrial algae need sunlight as energy source, and they are able to live in "extreme" environments. As they are autotrophy, they can synthesise they own molecules and also inorganic substances, such as carbon dioxide, water and some elements, and thereby obtain organic substances that guarantee their long-term survival, by means of photosynthesis and transforming light energy into chemical energy [42,55].

The algae which can be found on building façades are mostly green-algae, belonging to the division Chlorophyta [56–59]. Depending on the species, their size can range from few micrometres to few hundreds of micrometres. Their cells contain chloroplasts, that give their typical green colour. They can only live in environments with high humidity and sufficient but not too intense illumination. If exposed to favourable conditions they can proliferate very fast. On building, these algae usually form light or very dark green stains on the façade [42].

Cyanobacteria are also called blue-green algae (Cyanophyta). Some species of cyanobacteria possess well developed sheath layers around their trichome: thanks to UV-sunscreen pigments and secretion of copious extracellular polymeric substances (EPS), they are protected against desiccation and intense solar radiation. Indeed, cyanobacteria can survive even during the summer period and when the temperature on a building façades exceeds 60°C, coupled with high light intensity and extreme dryness [60–62].

2.4 Essential factors for algae growth

As for all other biological habitats the microorganisms are dependent on different biotic and abiotic factors for their growth on façades [42]. Different algal species have very different appearances, life-styles and tolerance of variations in temperature, moisture etc. and they are metabolically active when appropriate combinations of dampness, warmth and light are present [45,46,51,63]. Façades are characterized by extreme fluctuations of temperature, repeated desiccation and high UV-radiation: therefore, any organism living here must be able to tolerate these variations to maintain the metabolic activity [42].

In general, there is a lack of a deep knowledge about conditions which influence algae and cyanobacteria growth, but some common demands can be specified. For photosynthesis process the combination of sufficient light, water, temperature, carbon dioxide and some

mineral nutrients must be present. Algae can find also nutrients in some trace elements (Fe, Mn, Si, Zn, Cu, Co, Mo, B, V) for growth, which are normally available in the environment (rain, dust, material substrate), so that the local micro climate is the determining factor for biological growth on façades [64].

Several researches demonstrated that the algal growth is influenced by the substrate characteristics [20,48,65–70]. However, up to now they only revealed the role of some physical parameters of the substrate: porosity helps the retention of water and nutrient important for the growth of algae, while roughness favours the mechanical grip of algae to the substrate itself [65,67,70]. Neither the influence of pH action on algae is not well known, because it depends on the tolerance of each specific strain. Microorganism can be classified into acidiphiles, neutrophiles and basiphiles, but there also exist indifferent microorganisms which normally develop in a wide range of pH, such as bacteria whose growth is satisfactory between pH values equal to 6.0 and 9.0. However, it's known that most algae and cyanobacteria found on building façades can normally develop at a pH equal to 8.0 [55,71].

As photosynthetic organisms, algae and cyanobacteria need light and carbon dioxide to permit photosynthesis biochemical process and produce energy needed for maintenance, growth and reproduction [42,71,72].

Nevertheless, humidity and temperature are the most important environmental conditions that affects the growth. For each species of microorganism, an optimal temperature for growth and a range between a minimum and a maximum outside of which growth is not possible can be individuated [71]. According to literature, for most algae and cyanobacteria an optimal temperature for growth was estimated within the range of 20 °C and 30 °C [71,73,74], while the range of suitable growth is usually considered between 5 °C and 40 °C [75,76]. However the resistance to high temperatures (above 50 °C) or low temperatures (below 0°C) appreciably varies from one type of microorganism to another [61,62,77]. Under dry conditions algae can withstand extreme thermal conditions (heat or cold stress) much better than in humid conditions [64].

Water is necessary for algae growth as it is required for the photosynthesis. The water uptake directly occur through the cell wall by osmosis and the growth limit for some green and blue algae is about 100% RH (corresponding to liquid water) [75]. Wind driven rain and dew water are the main causes for wetting of façades with liquid water [36,78,79]. The geometry of the building may offer preferential routes where the water accumulated after a rain event stagnates, creating the ideal conditions for the proliferation of algae and cyanobacteria. If balconies or roof overhangs reduce the wind driven rain on the walls, a light inclination of the façade increase the surface exposed to the water [79]. Once the algae have grown, the run-off rain water contributes to replacing the old cells with new cells, and favours the spread of spots of biofilm to other non-contaminated building components [36].

However, algae and cyanobacteria can survive dry periods and can restart their growth when enough humidity is available. Therefore, a drying of façades during the day is not sufficient to prevent algae growth [64].

Chapter 3

Theory and equations

3.1 Avrami's theory and the existing predictive model

Only few studies have attempted to provide models aimed at describing and predicting algae biofouling on building materials. Preliminary investigations started with the development of a numerical simulation of biofilm growth in porous media [80]. Biofilm growth was implemented on irregular domain and substrate of any thickness were considered as independent parameter. Subsequently, solid substrate, were taken into account: the algal biofouling was calculated through a mathematical modelling which takes advantage of a system of nonlinear hyperbolic-elliptic partial differential equations [81,82]. This set of equations was implemented by considering illumination and temperature effects [83].

It was found that the physical phenomenon of growth and multiplication of algal cells generally follow a trend similar to a sigmoid curve [19]. Indeed, the growth of a micro-algae culture is characterized by three phases: an initial lag phase during the so-called "latency time" (when algal stains are not still visible), a phase of rapid growth and a final stagnation phase, when the covered surface by microorganisms become constant over the time (Figure 3.1) [66,67].

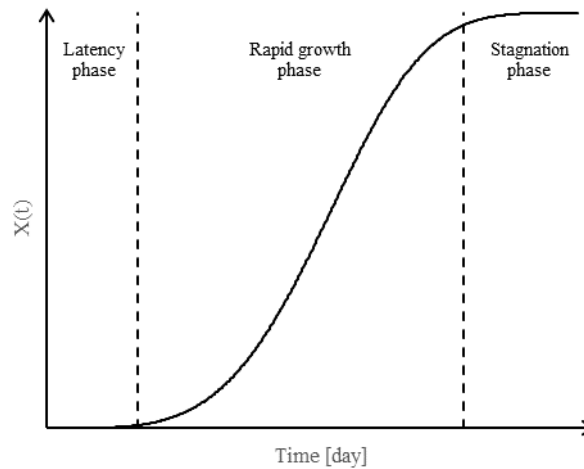


Figure 3.1. Typical growth of a micro-algae culture.

The work of Ruot and Barberousse showed a preliminary application of Avrami's theory for simulating the algal colonisation process as temporal evolution, but it lacked the kinetic process [18]. Then, the algal biofouling was numerically simulated [19–21], and it was found that Avrami's theory can correctly reflect the biofouling process under accelerated

laboratory growth conditions. Avrami's law has been developed in the form of an exponential equation by Avrami, Johnson and Melh [84–87]. This law was originally use to describe the kinetic phase transformation in solids [88,89], even if it is used in different fields: crystallization of polymers, heat treatment, decomposition of solids [90,91]. The Avrami's theory is based on two processes: the nucleation, which corresponds to the appearance of nuclei of a new phase, and the subsequent growth, which represents the increase in the size of these nuclei into the initial phase during time.

Likewise, also the biofouling process on building materials can be described by these two phases. Algal colonization starts with the attachment of algae on the substrate. Initially, algae appear as small green spots, which correspond the nuclei of the Avrami's model [19], then they grow increasing in size and forming algal filament increasing the covered extension on the material surface.

In order to represent the growth process also in case of non-complete biofouling, the original Avrami's law was improved into a modified model [20–22] described by the equation (1):

$$X(t) = (1 - \exp^{-K(t-t_1)^n}) \cdot \frac{A_c}{A_t} \quad (1)$$

where the covered area $X(t)$ [-] is given as a function of time t [day]. The rate coefficient K [-] is a parameter related to the growth rate and it is constant for each material. The time t_1 [day] represents the latency time before a chromatic variation occurs on the material surface. The Avrami's exponent n [-] is a coefficient which can be reasonably assumed equal to 4 in case of algae growth: three dimensions represents the growth and one represents nucleation rate assumed as constant [19,22,92]. Lastly, the final covered area ratio, indicated as A_c/A_t [-], expresses the percentage of covered area at the end of the growth process. A_c is the covered area by algae at the end of the accelerated growth test, and A_t is the total area of the sample exposed to biofouling [22].

The parameter K depends on the nucleation rate of algal cells and it is related to material properties. It can be calculated from equation (2):

$$K = \Lambda \cdot k_g \cdot k_c^2 \quad (2)$$

where k_g [spot/ μm^2 day²] is the specific attachment rate constant, indicating the rate of the nucleation of new particles, and k_c [$\mu\text{m}/\text{day}$] is the specific growth rate constant. The Avrami's constant Λ [-] can be determined by equation (3):

$$\Lambda = \frac{2}{(q+1) \cdot (q+2) \cdot (q+3)} \quad (3)$$

with:

$$q = n - 3 = 1 \quad (4).$$

The specific attachment rate constant k_g can be obtained by linear regression from the specific attachment rate $d\gamma/dt$ [spot/ μm^2 day], which defines the number of algal spots that appears on a surface unit per time unit (equation (5)):

$$\frac{d\gamma}{dt} = k_g \cdot (t - t_1)^q \quad (5)$$

where γ is the number of algal spots at time t per unit area [Spot/ μm^2].

On the contrary, the growth rate constant k_c can be experimentally determined by calculating the equation (6):

$$k_c = \frac{\sqrt{S_{t+\Delta t}} - \sqrt{S_t}}{((t + \Delta t) - t)} \quad (6)$$

where S_t [μm^2] represents the area of an algal spot at time t , and $S_{t+\Delta t}$ [μm^2] is the area of the same algal spot at time $t+\Delta t$.

The modified Avrami's model (equation (1)) for the biofouling modelling was validated by several researches [20–22]. Moreover, a recent study demonstrated a good correspondence between the K parameter analytically determined by least square method and the one experimentally calculated by digital image analysis (DIA) [22]. The model also highlighted the role of the substrate, and in particular referring to porous structure and roughness properties. For high porous and high rough materials, the substrate promotes the water availability inside the material and the adherence of microalgae to the substrate itself, thus increasing the colonization rate and leading to a rapid coverage of the surface by algae [69].

Even if it is known the influence of the substrate, the effect of environmental conditions is still totally missing. Furthermore, the equation (1) of the modified Avrami's model does not actually give the possibility to directly introduce as variables neither the substrate properties nor the environmental conditions. A new failure model which explicitly includes parameters and allow to predict the algae biofouling over the time, is thus needed.

3.2 New failure model based on the Avrami's law

The proposed failure model derives from the modified Avrami's model (equation (1)) by making explicit the influencing parameters that mostly regulate algal growth and development on different building materials. Equation (7) shows the proposed failure model:

$$X(P, R, A, T, RH, t) = \Omega \cdot \tau_A \cdot \frac{A_c}{A_t} \cdot \left[1 - \exp^{-(\tau_K \cdot K)(t - \tau_l \cdot t_1)^n} \right] \quad (7)$$

where the covered area X [-], the final covered area ratio A_c / A_t [-], the growth rate K [-] and the latency time t_l [day] refer to the same parameters of the modified Avrami's model (equation (1)), while Ω [-] and τ_A , τ_K and τ_l [-] are new scale functions introduced to take

into account also the effect of the environmental conditions. The Ω function characterises the effects of RH on the covered area, while the τ_i values represent the effects of temperature and substrate on each corresponding parameter A_c / A_t , K and t_1 .

The equation (7) is a function of time t [day], of substrate properties (total porosity P [%], roughness R [μm] and total pore area A [m^2/g]), and of environmental conditions (temperature T [$^\circ\text{C}$] and relative humidity RH [%]). These variables were chosen and included into the general equation of the failure model in order to be independent variables, based on previous studies which have investigated the algal development on building materials [23,48,51,65]. From these works indeed, it can be noted that porosity is responsible for water availability, e.g. high porous materials can retain high amount of water while for low porous materials water availability is reduced [20,66,70,93]. Moreover, the total pore area affects the water adsorption and desorption capacity [23]. Roughness, instead, favours the mechanical adhesion of cells to the surface micro-indentations and small irregularities of substrate [20,70]. Temperature can alter the biofouling process [73,75,94], influencing the growth rate and the percentage of covered area, while relative humidity can have effect on the free water available inside the porous structure of the sample [23,36,50].

Furthermore, the eventual secondary effects of other substrate properties (e.g. surface pH, nutrients and salts [65,78]), are introduced as corrective coefficients (α , ..., μ), both for parameters and scale functions. They are related to the different nature of the building materials, such as i.e. bricks, sandstones and limestones (see Section 5.2.2).

In the set of equations (8) for each term of equation (7) the investigated variables, regarding the material properties and/or the environmental conditions, are shown.

$$\left\{ \begin{array}{l} \frac{A_c}{A_t} = \frac{A_c}{A_t}(P, R, A) \\ K = K(P, R, A) \\ t_1 = t_1(P, R, A) \\ \Omega = \Omega(RH, P, R, A) \\ \tau_A = \tau_A(T, P, R, A) \\ \tau_K = \tau_K(T, P, R, A) \\ \tau_{t_1} = \tau_{t_1}(T, P, R, A) \end{array} \right. \quad (8)$$

The model follows the following three assumptions.

- First assumption: the substrate properties P , R and A do not depend from time t , as they are constant during time for a given material. This can be considered a good approximation, if aging problems of the building material surface can be disregarded. On the contrary, T and RH they are environmental conditions that obviously change as function of time.
- Second assumption: the variables P , R , A , and RH are considered as independent variables: this also means that the substrate properties P , R and A do not depend from each other and form the environmental temperature T . (These statements can be reasonably assumed from the experimental results, see Section 6).
- Third assumption: the covered area by algae $X(t)$ is a monotonically not decreasing function. Therefore, even if there are not suitable environmental conditions for algae growth, the biofouling process can never get back to a less contaminated stage. This assumption was supported by the results obtained in previous experimental researches [20–22], from which the condition (9) was always valid.

$$X(t_1) \leq X(t_2), \quad \forall t_1 < t_2 \quad (9)$$

According to the above hypotheses, the failure model manages to simulate the algae growth on a specific building material, taking into account also the environmental conditions that change over time. Figure 3.2 presents a qualitative example. In Figure 3.2a, the calculation process is shown: once set the substrate properties, the biofouling is influenced only by the environmental conditions over the time. Hence, the model determines the specific growth curves for the different environmental conditions: in this case, the growth process is hypothesized to be influenced by three different climatic conditions (EC_i , $i=1,\dots,3$). During each time interval, the model identifies the section of the curve related to EC_i (Figure 3.2a). Finally, the overall growth process in terms of area coverage under variable environmental conditions is the sum of each section, as shown in Figure 3.2b.

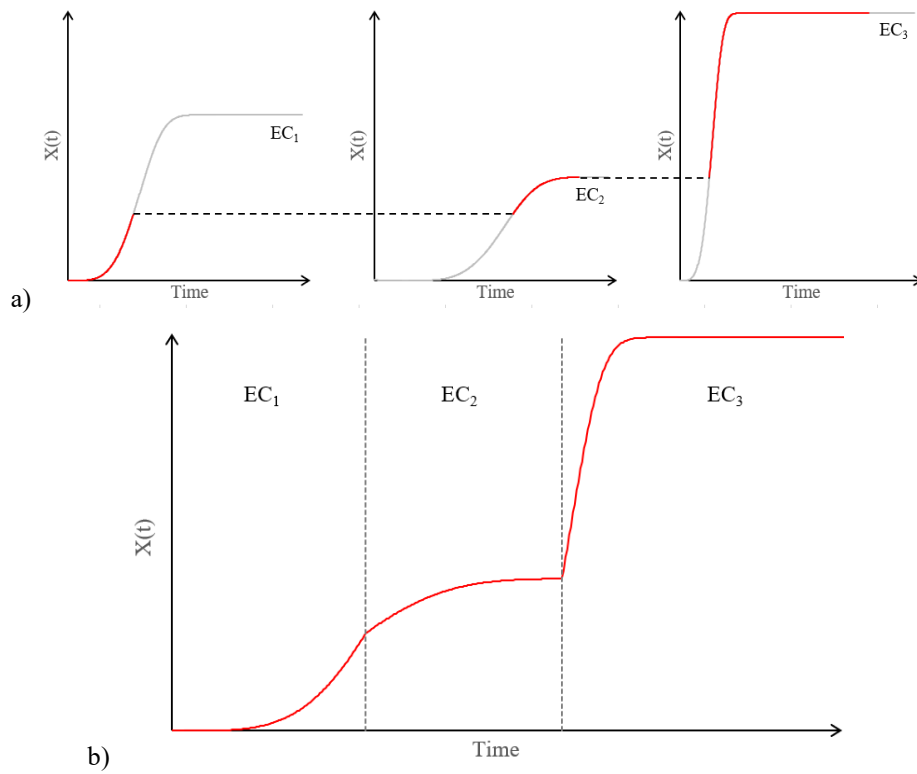


Figure 3.2. A qualitative example of the implemented failure model: a) determination of the growth curve under each exposure condition; b) the overall process of covered area by algae biofouling under variable environmental conditions over the time.

Chapter 4

Experimental program

The experimental program was defined according to the assumptions about the definition of the failure model, listed in Section 3.2. In particular, the tested materials and the environmental conditions T and RH , set during the performed tests, were chosen in order to be independently treated in the mathematical model [95].

Generally, the study of biofouling on building materials may raise some methodological problems concerning its occurrence as readily observable and quantifiable phenomenon [96]. In fact, a visible biological deterioration usually starts after 1-year or more of natural exposure [97,98], and for this reason the use of accelerated tests is generally recommended. In literature it is possible to find a large variety of tests apparatus based on wet&dry cycles [70,99–105]. The accelerated growth tests performed in this research are reported in Section 4.4 and in Section 4.5.

The experimental activity was mainly carried out following three steps of investigations. In the first step (see Section 4.3), preliminary tests under different constant temperatures were carried out, to investigate the temperature effect merely on algae growth (without considering the brick substrate). The aim of this first investigation was to select the environmental temperatures to set during the following accelerated growth tests on building materials. In the second step (see Section 4.4), tests focused on the effect of different relative humidity conditions (RH _tests) under a constant temperature (Table 4.1), previously selected according to the preliminary tests results. In the third and last step (see Section 4.5), tests were aimed to the investigation about the role of temperature (T _tests) under a constant relative humidity (Table 4.1).

| Test | Temperature [°C] | Relative Humidity [%] | |
|----------------|---------------------|--------------------------|------------------------------|
| Reference_test | Test_0 | 27.5 ± 2.5 | ≥ 98 , wet & dry cycles |
| RH _tests | Test_1 | 27.5 ± 2.5 | 75 ± 2 |
| | Test_2 | 27.5 ± 2.5 | 87 ± 2 |
| | Test_3 | 27.5 ± 2.5 | 98 ± 2 |
| T _tests | Test_4 | 5 ± 2.5 | ≥ 98 , wet condition |
| | Test_5 | 10 ± 2.5 | ≥ 98 , wet & dry cycles |
| | Test_6 | 40 ± 2.5 | ≥ 98 , wet condition |

Table 4.1. Environmental conditions during the accelerated growth tests on building materials.

Table 4.1 lists the tested environmental conditions set during the accelerated tests. All the tests performed in previous works [20–22,106,107] were grouped in the Reference Test, since temperature and relative humidity belonged to the range of the optimal algal growth, that is in a temperature between 20 °C and 30 °C [71,73] and with the presence of free water [51,65].

To monitor the environmental conditions set inside each growth chamber during the tests, temperature and humidity Sensirion SHT31-D sensors were connected to a National Instruments (NI) myRIO-1900 data logger device (Figure 4.1a). Sensors features are reported in Table 4.2.

| Measurement | Specification | Value | Unit |
|-------------------|--------------------|------------|------|
| Relative humidity | Accuracy tolerance | ± 2 | % RH |
| | Specified range | 0 to 100 | % RH |
| Temperature | Accuracy tolerance | ± 0.3 | ° C |
| | Specified range | -40 to 125 | ° C |

Table 4.2. SHT31D sensor performance specifications.

Thanks to the small dimensions of the sensors (12,5 x 18 x 2,6 mm) it was possible to locate them near the samples. The exposed delicate parts of sensors and electric contacts were protected with silicon from vaporized water (Figure 4.1b). The monitoring system was previously tested and calibrated in other researches, aimed to characterize building materials and investigate the critical conditions in terms of high moisture loads in the environment, i.e. of a hypogean environment [108–111], and in a thermal retrofitted building, at the interface between the insulation system and a historic masonry wall [112]. All measurements were recorded every 10 minutes and collected data were constantly monitored to avoid malfunctions of the system and ensure not to compromise the algae growth process.

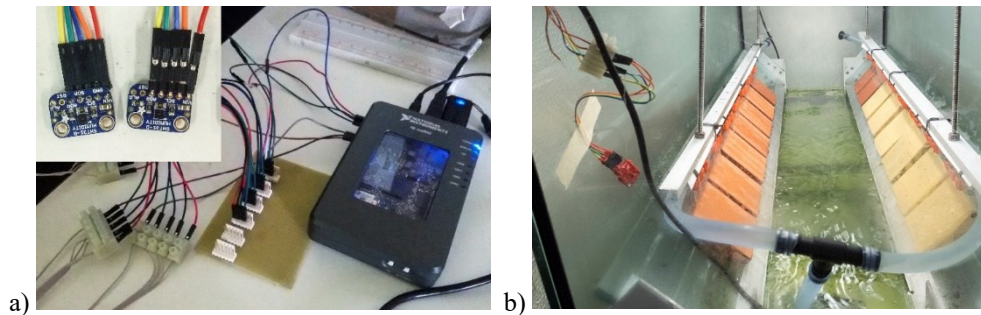


Figure 4.1. a) Assembled measurement system with SHT31-D sensors and NI myRIO-1900 data logger; b) Protected T/RH sensor positioned near the samples inside a growth chamber during the accelerated tests.

4.1 Algae cultures

The microbial cultures chosen for the experimental tests were a green alga (*Chlorella mirabilis* strain ALCP 221B) and a cyanobacterium (*Chroococcidiopsis fissurarum* strain IPPAS B445), since they can be commonly found on building façades, especially in European countries [44,48,51,56,97,103,113,114]. The microbial strains were cultivated as pure cultures in 5-L glass flasks containing Bold's Basal medium (BBM), prepared in accordance with ASTM D5589-09 standard method [115]. The recipe for Bold's Basal Medium, which supports the growth of a wide range of algae, is given in Table 4.3. To obtain 1 L of BBM, 10 mL of each stock solution 1 through 6 were combined with 1 mL of stock solution 7 through 10 in 936 mL of distilled water.

| No. | Stock solutions | g/400 mL |
|--------------------------|---|----------|
| 1. | NaNO ₃ | 10 |
| 2. | MgSO ₄ · 7H ₂ O | 3 |
| 3. | NaCl | 1 |
| 4. | K ₂ HPO ₄ | 3 |
| 5. | KH ₂ PO ₄ | 7 |
| 6. | CaCl ₂ · 2H ₂ O | 1 |
| Trace elements solutions | | g/L |
| 7. | ZnSO ₄ 7H ₂ O | 8.82 |
| | MnCl ₂ 4H ₂ O | 1.44 |
| | MoO ₃ | 0.71 |
| | CuSO ₄ 5H ₂ O | 1.57 |
| | Cu(NO ₃) ₂ 6H ₂ O | 0.49 |
| 8. | H ₃ BO ₃ | 11.42 |
| 9. | EDTA | 50 |
| | KOH | 31 |
| 10. | FeSO ₄ 7H ₂ O | 4.98 |
| | H ₂ SO ₄ O | 1 mL |

Table 4.3. Composition of the stock solutions used for the preparation of the BBM (Bold Basal Medium).

Both cultures were incubated at 24 °C providing the needed illumination with a light intensity of 1500 lux and a 14/10 h light/dark photoperiod. The mixed cultures to be used in the experimental assays were obtained by mixing the two pure cultures in a ration 1:1 (v/v) (Figure 4.2).

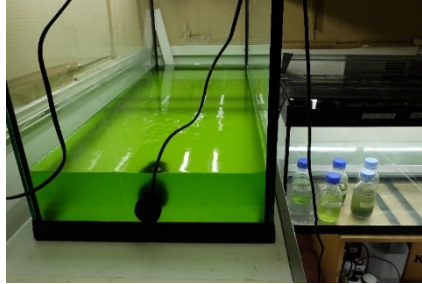


Figure 4.2. Mixed microalgae suspension of *Chlorella mirabilis* and *Chroococidiopsis fissurarum* after incubation.

4.2 Tested building materials

In this research algae biofouling was evaluated on different building materials. Investigations were carried out on fired bricks and stones, since these materials are usually found on façades, and especially in Cultural Heritage [116,117].

According to previous literature works, fired brick samples were considered [20,21,95,106]. Nine different types of fired bricks (named B) were selected and they were cut into three prismatic samples with dimension equal to $8 \times 8 \times 3 \text{ cm}^3$ (Figure 4.3a). They were chosen considering their different total porosities P and total pore areas A , as reported in Table 4.4. In addition to the porous structure, also different levels of roughness R were examined. A smoothing treatment with sand paper was manually applied on some samples. Treated samples were identified with “S”, while samples with original surface roughness were named with “R” at the end of the acronym. Material B-1 and B-4 refer to previous investigations on algae biofouling [20,21,106].

| Sample | Total porosity P [%] | Roughness R [μm] | Total pore area A [m^2/g] |
|--------|---------------------------|------------------------------------|--|
| B-1S | 19.13 ± 1.66 [21] | 2.4 ± 0.5 [21] | 6.19 ± 0.97 |
| B-1R | 19.13 ± 1.66 [21] | 2.8 ± 0.5 [21] | 6.19 ± 0.97 |
| B-2S | 19.24 ± 0.37 | 4.50 ± 0.27 | 6.19 ± 1.18 |
| B-2R | 19.24 ± 0.37 | 5.54 ± 0.42 | 6.19 ± 1.18 |
| B-3 | 24.62 ± 1.02 | 2.95 ± 0.63 | 2.22 ± 0.21 |
| B-4S | 36.65 ± 0.65 [21] | 1.1 ± 0.1 [21] | 2.21 ± 0.31 |
| B-4R | 36.65 ± 0.65 [21] | 8.9 ± 0.9 [21] | 2.21 ± 0.31 |
| B-5S | 44.09 ± 1.63 | 6.60 ± 0.49 | 5.57 ± 0.83 |
| B-5R | 44.09 ± 1.63 | 7.60 ± 0.57 | 5.57 ± 0.83 |

Table 4.4. Substrate properties of tested fired brick materials (mean value \pm standard deviation). In brackets references of previous works are reported.

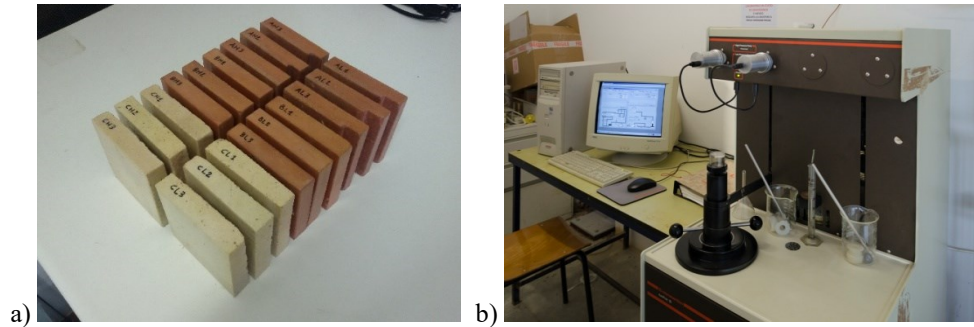


Figure 4.3. a) Brick samples prepared for the experimental investigations;b) Mercury intrusion porosimetry for the characterization of the sample substrates.

Concerning stone materials, two different types of sandstone (named S) and two types of limestone (named L) were considered, referring to previous researches reported in literature [22,107], which investigated the algae growth adopting the same methodology. The characteristics of the stone substrates (Table 4.5) significantly differed from the brick ones. In particular, all of the tested samples were characterized by a lower porosity (lower than 20%). These stone samples were not manually smoothed.

| Sample | Total porosity P [%] | | Roughness R [μm] | | Total pore area A [m^2/g] |
|--------|---------------------------|------|------------------------------------|------|--|
| S-1 | 4.52 ± 0.18 | [22] | 7.9 ± 0.4 | [22] | 1.67 ± 0.19 |
| S-2 | 7.74 ± 0.26 | [22] | 7.6 ± 0.6 | [22] | 1.76 ± 0.17 |
| L-1 | 7.54 ± 0.31 | [22] | 2.0 ± 0.1 | [22] | 2.54 ± 0.22 |
| L-2 | 18.17 ± 0.46 | [22] | 2.6 ± 0.2 | [22] | 3.92 ± 0.28 |

Table 4.5. Substrate properties of tested stone material (mean value \pm standard deviation). In brackets references of previous works are reported.

To evaluate the effect of the substrate, the clay brick and stone materials selected for the experimental investigations were preliminarily characterized before the tests. Total porosity P [%] and total pore area A [m^2/g] of each material were determined onto 3 samples by a mercury intrusion porosimeter (Micromeritics Autopore III) (Figure 4.3b) following the ASTM D4404-10 standard [118].

The surface roughness, as arithmetical mean roughness R_a [μm], was determined according to UNI EN ISO 4287:2009 standard [119], by using a Taylor Hobson CCI 3D Optical Profiler (Figure 4.4). The arithmetical mean deviation of the assessed profile was calculated on five sampling lengths of 5,54 mm.

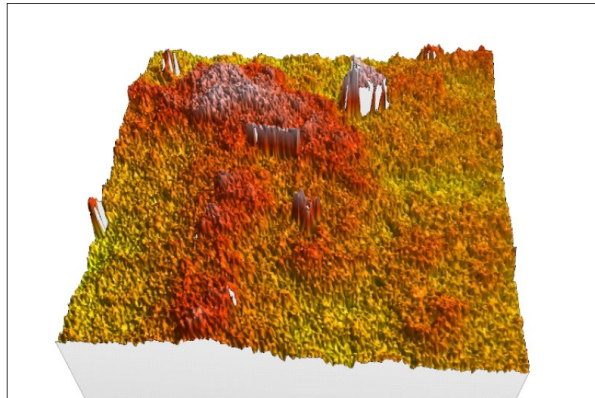


Figure 4.4. Magnification of a brick surface (sample B-2R) by the optical profiler for roughness determination.

4.3 Preliminary tests about the influence of temperature on algae growth

As preliminary investigations before the accelerated tests, the effect of five different temperatures were analysed, evaluating the growth rate of algae cultures, without considering the material substrate. The aim of this preliminary tests was to understand the suitable temperatures to set during the accelerated tests on brick samples, in order to obtain useful results for the implementation of the failure model, and not to waste time in non-favourable environmental conditions for growth [95].

According to the available literature, algae can live in a wide range of temperature, which are usually comprised between 5 and 40°C [75,76]. Considering this range, algal cultures were incubated at the following temperatures: 5°C, 10°C, 27.5°C, 35°C and 40°C. The set temperatures were maintained with the accuracy of $\pm 2.5^\circ\text{C}$. Both temperature and relative humidity were measured with digital sensors (Sensirion SHT31-D) positioned inside each incubator (see Section 4.2).

Growth tests were carried out on both pure and mixed cultures, using glass bottles containing 100 mL of each culture, incubated in a refrigerated thermostat (Velp FOC 215E) and in a controlled room with constant temperature (Figure 4.5a). Since algal cells need sun light to reproduce, a controlled daylight with an intensity of 1500 lx was provided for day/night cycles of 14/10 h., by installing two 39 W neon lamp (Sylvania TopLife, 5000 K light temperature) inside the growth chamber [42]. Every week the cultures were sampled and a microscopy count was carried out using a Thoma-Zeiss hemocytometer (Figure 4.5b) [120]: the results were expressed in logarithmic scale as number of cells/mL. All the tests were performed in duplicate.

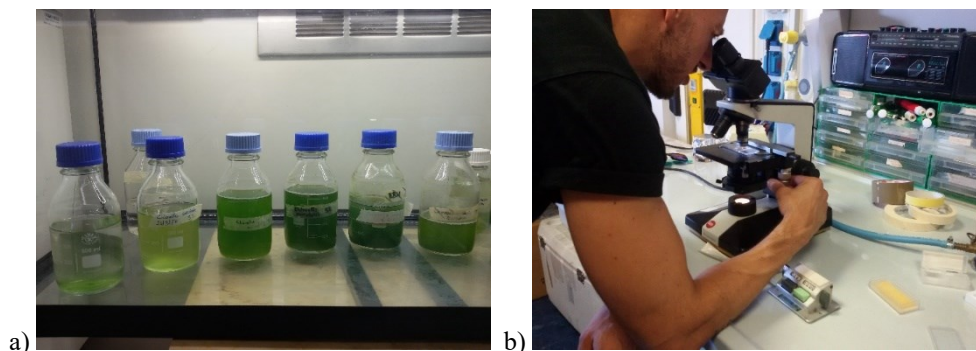


Figure 4.5. a) Algae cultures were incubated in controlled environment under different constant temperatures; b) Counting of the number of cells of the tested cultures in a Thoma-Zeiss hemocytometer under a light microscope.

4.4 Accelerated growth tests under different constant relative humidities

In order to evaluate the influence of relative humidity on the growth of algae on fired brick surfaces, three tests (Test_1, Test_2 and Test_3) were carried out (see Table 4.1) [95]. Three different relative humidity (RH_i) conditions were reproduced inside three separate climatic chambers. The air of the indoor environment was conditioned by using different saturated solutions, following the methodology of reported in EN ISO 12571:2013 [121].

The three incubators consisted of $100 \times 40 \times 53$ cm³ glass chambers, each one filled with 15L of saturated solution (Figure 4.6a). The RH_1 ($75 \pm 2\%$) was obtained through a saturated solution of NaCl, RH_2 (about $87 \pm 2\%$) through a saturated solution of Na₂CO₃, and RH_3 (about $98 \pm 2\%$) through only deionized water [122]. To exclusively evaluate the effect of relative humidity, during all the tests temperature was constantly controlled and maintained at $27.5 \pm 2.5^\circ\text{C}$ (see table Table 4.1). This temperature was selected considering the results of the preliminary tests (see Section 6.1), aimed to individuate an optimal temperature for growth in accordance with literature [71,73,74]. Environmental conditions inside each glass chamber near the samples were constantly monitored and measurements were recorded every 10 minutes over the entire test period (see Section 4.2).

For each tested material three prismatic samples ($8 \times 8 \times 3$ cm³) were prepared. The behaviour of the sample put in each environment were investigated until the end of a possible biofouling process (stagnation phase) was reached. At the beginning of each test, samples were inoculated on 9 different points on their surface with 5 μL of the mixed culture per point. After the initial inoculation, samples were placed inside the climatic chambers, on aluminium-glass racks inclined at 45° , and positioned front-to-front along the long dimension of the chamber. All the three growth chambers were placed in a dark room to avoid the influence of the external environment (daily light, outdoor temperature and relative humidity). Each test apparatus was equipped with two neon lamps (Sylvania TopLife 39W) to provide an adequate illumination to simulate a day/night cycles of 14/10 h [42]. The lamps

were positioned on the top of the chamber at a constant distance from the sample surface (Figure 4.6b).

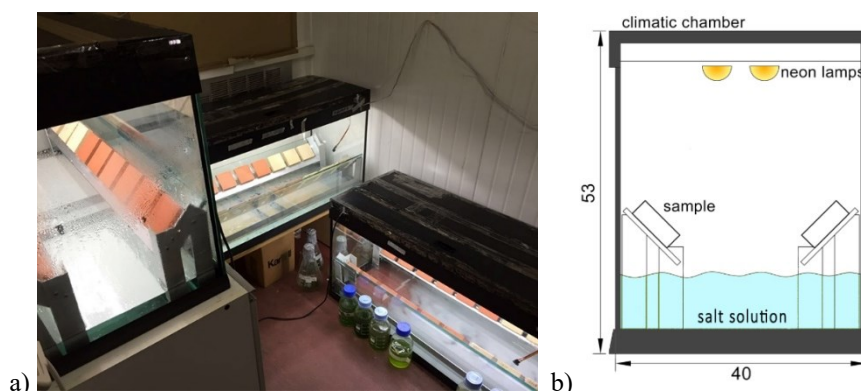


Figure 4.6. a) View of the glass chambers used to maintain different constant relative humidities; b) Scheme of the test apparatus build up for investigations on relative humidity effect.

4.5 Accelerated growth tests under different temperatures

Investigations on the effect of temperature on algae growth were carried out following the methodology adopted in previous researches [20,21,69,95,105]. The method well simulates the behaviour of roof or external wall surfaces exposed to “bad weather”, or leaky parts of a building or design defects. It consists in accelerated tests with periodical water spray on the material surface. Tests were performed until the biofouling on each sample reached the stagnation phase at the end of the growth process [95].

Different growth chambers ($100 \times 40 \times 53 \text{ cm}^3$) were filled with 35L of BBM and microbial suspension, composed by a mix of the two algal strains (see Section 4.1), in a concentration of about 4mg of algal cells per litre. The broth culture was continuously agitated with two wave pumps (Hydor, model Koralia 1600/425) positioned at the base of the glass chamber. The glass chamber was equipped by two aluminium-glass racks inclined at 45° on which the samples were positioned. Above each rack, a PVC tube, with three holes drilled every 20 mm in correspondence of each sample, was connected to a 500 L/h water pump (Blupower) submerged in the broth culture. That way, the algal suspension was sprinkled on sample surfaces ($8 \times 8 \text{ cm}^2$), falling down their entire surface with run/off cycles of 15 minutes, for a total duration of 6 hours per day (3 hours run and 3 hours off). The distance from the samples to the rails to was approximately 50 mm and designed to allow water to run on the entire sample surface (Figure 4.7a).

Tests were carried out inside a closed room to avoid the influence of outdoor environment. Cycles of day/night illumination (14/10 h) were provided by installing two 39 W neon lamps with a light temperature of 5000 K (Sylvania TopLife) under the lid of the growth chambers (Figure 4.7b). During the light period of 14 h, the solar light lamps were switched on, while for the remaining 10 h, all the lamps were turned off to simulate the night period.

According to the results about the different temperatures tested in the preliminary experiments (see Section 4.3) and considering the available literature [21,71,73–76,94,123], the accelerated tests were set under two different temperatures. A temperature of $27.5 \pm 2.5^\circ\text{C}$ was selected to be within the range of the optimal growth conditions comprised between 20°C and 30°C [21,71,73,74,94,123], and a lower temperature of $10 \pm 2.5^\circ\text{C}$, within the range of suitable growth for both the studied strains [75,76]. A modified refrigerator Electrolux RC 5200 AOW2 was used to set the lower test temperature. In these experiments, relative humidity was assumed equal to 100%, since the wet&dry cycles allow to keep the sample surface wet during the test time. Temperature and relative humidity sensors were used to monitor all the test environments, through measurements taken every 10 minutes (see Section 4.2).

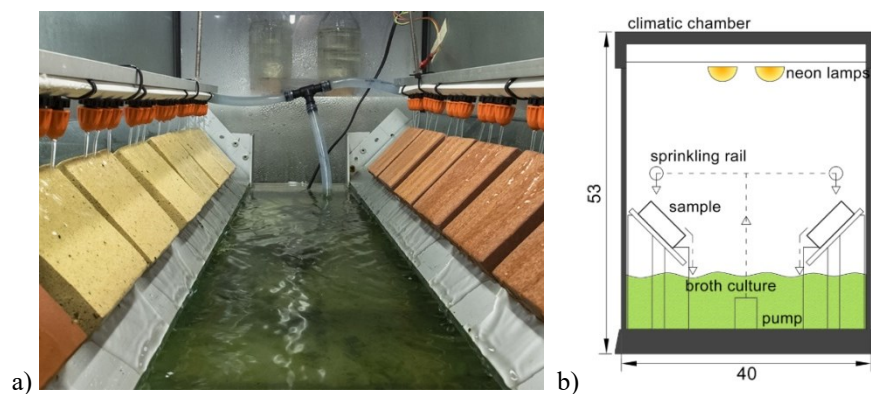


Figure 4.7. a) View of the inside growth chamber used for the evaluation of temperature influence on algae biofouling; b) Scheme of the run-off test apparatus built up for the accelerated tests.

4.6 Measurement and evaluation of algae growth

Two different techniques were adopted to investigate the algal growth on the tested samples. During the accelerated growth test, the evaluation of the biofouling process and the algal extent on samples' surface were carried out by both qualitative and quantitative analyses [69,95,105,107].

Qualitative analyses were performed by chromatic investigations during the tests. Colorimetric measurements for the evaluation of the chromatic variation (ΔE) were carried out using a portable spectrophotometer (Konika Minolta CM-2600d) [99,105] (Figure 4.8a). In accordance with UNI EN 15886:2010 and UNI 1602371:2018, an aperture of 3 mm, a CIE standard daylight illuminant (D65) and an observer field size angle of 10° were set [124,125]. On each sample surface, nine measurements were weekly repeated on the same points. In order to guarantee the replication of measurements on the same points in subsequent tests, a reference spatial grid (8×8 cm) was used.

Results were averaged to obtain a representative value for each material and they were expressed in CIELab colour space [89]. Colour variations were calculated in terms of total colour difference ΔE , following the equation (10):

$$\Delta E = \sqrt{(L_0^* - L^*)^2 + (a_0^* - a^*)^2 + (b_0^* - b^*)^2} \quad (10)$$

where L_0^* , a_0^* and b_0^* indicate the colour coordinates of samples at time zero (prior the start of the test), and L^* , a^* , b^* the coordinates measured during the tests. According to standard methods [125] and researches [126], a total colour difference $\Delta E < 1$ can be considered not visible by naked human eyes. On the contrary a ΔE ranging between 1 and 2 can be detectable only with a close observation. From an engineering point of view, a $\Delta E = 1$ could be assumed as the acceptable lowest limit for algae growing. In case of average $\Delta E > 1$, the term $a_0^* - a^*$ was then evaluated to verify if the colour change was actually due to the presence of algae. The variation Δa indicates to a colour difference in a red/green scale. That way, it permits to associate the colour variation to the appearance of algae as green stains: the amount of red is indicated by positive values ($\Delta a > 0$), while a green toning by negative values ($\Delta a < 0$). Thus, in case of average $1 < \Delta E < 2$ but at the same time average $\Delta a > 0$, it can be reasonably assumed that the colour variation is not due to the presence of algae.

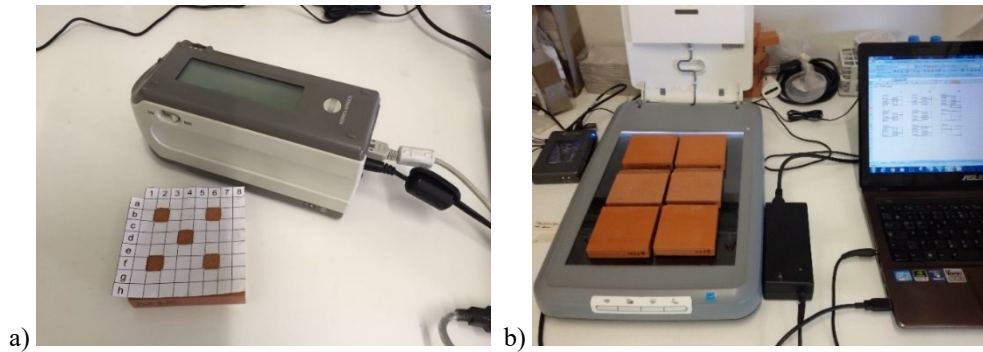


Figure 4.8. a) Colorimetric measurements on the same points of the samples' surface during the test; b) Digitalization of the samples' surfaces for the biofouling extent evaluation.

The colorimetric analyses were associated to the quantification of the biofouling extension, evaluated by a (quantitative) Digital Image Analysis (DIA). The effectiveness of this methodology has been widely confirmed in previous studies [65,69,100,101,104,107]. According to these researches, DIA is one of the easiest and non-destructive tests used to measure the algal growth [65,101]. In particular, to calculate the extension of colonized area the threshold method was adopted [65,69,104,107].

Samples' surfaces were weekly digitalized and, to this aim, a scanner HP Scanjet G3010 was used for the acquisition of high-resolution images (600 dpi resolution). The scanned images were elaborated to calculate the algal coverage, expressed as a percentage of the total sample area (Figure 4.8b). To identify the colonized area, the acquired images were processed with ImageJ software [127,128]. Once the threshold values in CIELab colour space were set, the acquired images were subjected to a binary conversion to exclude the uncontaminated

parts of the samples and count only the contaminated pixels by algal cells (Figure 4.9). The covered area by microalgae was represented by the amount of black pixels and it was expressed as a percentage: 0% corresponding to a null-growth, while 100% corresponding to a completed coverage of the sample surface [104]. The acquisition of the scanned images were performed once a week during the accelerated growth tests and results were reported as average values and standard deviations of three samples for each fired brick material.

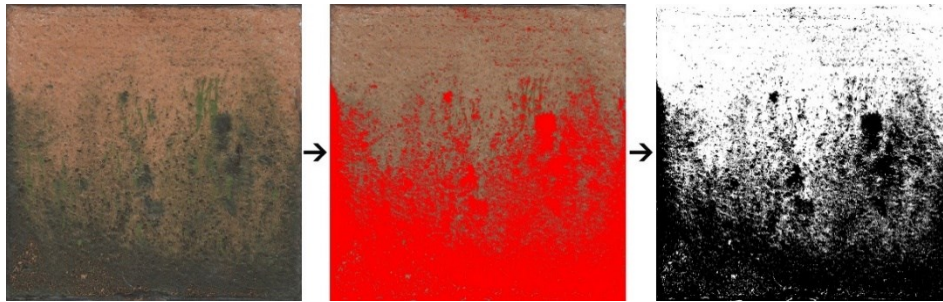


Figure 4.9. An example of binarization process; from left to right: scanned images from the original sample were elaborated by a filtering process (threshold method) to obtain binary images.

In addition to the above investigations, observations of brick surfaces using a scanning electron microscope (SEM) were carried out onto representative samples to have a better insight into the mechanical interactions among algae and cyanobacteria and the tested fired brick surfaces.

In order to preserve the biological material before SEM observation, all the brick surfaces were subject to the treatments proposed by Gao et al. [129] except for the post-fixation step with osmium tetroxide [130]. Briefly, a portion of selected bricks was fixed in 30 g/L glutaraldehyde in 0.1 M phosphate buffer, pH 7.0, for 4h at 25 °C. Samples were subsequently submerged in phosphate buffer for 15 min three times. Samples were dehydrated in ethanol at the following concentrations: 15%, 30%, 50%, and 70% for 10 min each, 85% and 95% for 15 min each, and 99.5% for 1 h. Samples were gold coated in a sputter coater K550X (Emitech, Ashford, United Kingdom). Finally, the brick portions were observed by using a XL30 SEM (Philips Amsterdam, Netherlands) equipped with a ES-423 extended life lanthanum hexaboride LaB6 cathode.

Chapter 5

Calculation methodology

5.1 Experimental determination of Avrami's parameters and scale functions

5.1.1 Experimental Avrami's parameters

After the acquisition of the scanned images of the samples' surface during the accelerated tests (see Section 4.6), the biofouling was modelled according to the modified Avrami's model (equation (1)). The parameters A_c/A_t , K and t_l were thus determined according to previous works [19–22,95]. The final covered area ratio, represented by A_c/A_t [-], was calculated at the end of the test measuring the covered area A_c by algae on the total area A_t of the sample (see Section 4.6). The rate parameter K [-] was determined, through iterations, by minimizing the least squares values between the experimental data and the values calculated with equation (1). The latency time t_l [day] corresponded to the time until $X(t) = 0.3\%$, as that guarantees the best reproducibility of the experimental results [21]. The parameters A_c/A_t , K and t_l were determined for each material as the average values of measurements on 3 samples. These values were then used as start values for the following implementation of the modified Avrami's formulation (equation (1)).

5.1.2 Experimental scale functions for the effect of environmental conditions

To quantify the scaling effect of temperature and relative humidity on the biofouling process, the value of τ_i and Ω were firstly experimentally determined from the results obtained after the accelerated growth tests.

The Ω values were determined according to equation (11). This equation expresses the normalization of the final covered area ratio $(A_c/A_t)_{Test_i}$, reached under the RHs tested (Test_0, ..., Test_3), by the $(A_c/A_t)_{Test_0}$ value reached under the relative humidity condition of the reference test (wet&dry cycles).

$$\Omega_i = \frac{(A_c/A_t)_{Test_i}}{(A_c/A_t)_{Test_0}}, \quad i = 0, \dots, 3 \quad (11)$$

Similarly, the τ_i values (respectively τ_A , τ_K and τ_{t_l}) were calculated according to equation (12). Scale functions τ_A , τ_K and τ_{t_l} respectively express the ratio between the experimental values of A_c/A_t , K and t_l , obtained under the different tested temperatures (Test_0 and Test_4, ..., Test_6), and the reference value obtained in Test_0 (with $T=27.5^\circ\text{C}$).

$$\left\{ \begin{array}{l} \tau_{Ai} = \frac{(A_c/A_t)_{Test_i}}{(A_c/A_t)_{Test_0}} \\ \tau_{Ki} = \frac{K_{Test_i}}{K_{Test_0}} \\ \tau_{t_i} = \frac{t_{1,Test_i}}{t_{1,Test_0}} \end{array} \right. , i = 0, 4, \dots, 6 \quad (12)$$

5.2 Analytical determination of Avrami's parameters and scale functions

According to the methods presented in this section, the equations of the set (8) were formulated as explicit functions of substrate properties and environmental conditions. The domain of each variable together with the codomains of both parameters and scale functions were determined; they are reported in Section 5.2.1. The method for the iterative fitting process is presented in Section 5.2.2.

5.2.1 Domains and codomains

For each variable of the equation set (8) the domains of the variables considered in this research were as follow, according to the physical range of the variables and the experimental methods:

- porosity domain is: $0 < P < 100$ [%];
- roughness domain is: $R \geq 0$ [μm];
- total pore area domain is: $A > 0$ [m^2/g];
- temperature domain is: $5 \leq T \leq 40$ [$^{\circ}\text{C}$];
- relative humidity domain is: $0 \leq RH \leq 100$ [%].

Moreover, the codomains of both parameters (A_c/A_t , K and t_l) and scale functions (Ω and τ_i) were set according to the mathematical and physical meaning, and considering the experimental results [20–22,106,107]; in particular:

- for the final covered area ratio: $0 \leq A_c/A_t \leq 1$ [-];
- for the rate parameter: $0 \leq K \leq 1$ [-];
- for the latency time: $t_l \geq 0$ [day];
- for relative humidity scale function: $0 \leq \Omega \leq 1$ [-];
- for temperature scale functions: $0 \leq \tau_i \leq 1$ [-].

5.2.2 Data fitting for the determination of the failure model equations

Each equation of the set (8) were determined by an iterative fitting process, based on data obtained both by literature researches [20–22,106,107] and the experimental tests (see Section 4) performed on fired brick materials.

Different types of equations were analysed and evaluated by combining regression coefficients (a, \dots, v) to the substrate (P, R and A) and environmental (T and RH) variables, in the parameters ($A_c/A_t, K$ and t_l) and scale functions (Ω and τ_i) of equation (7). The tested equation types (polynomial, logarithmic and exponential...) in the fitting process were not decided in advanced nor analytically derived from the starting equation (7). During the fitting process, the resulting equations were considered adequate if:

- the equation types well simulated the trend of the experimental data;
- the results of the equations along with the regression coefficients verified the codomains (see Section 5.2.1);
- the fitting maximised the coefficients of determination R^2 and minimised the sums of squared residuals.

The iterative process was stopped when all the above three conditions were satisfied. The regression coefficients (a, \dots, v) which resulted insignificant were discarded together with the relative variables.

The resulting equations and the regression coefficients determined for fired brick materials were then applied to stone materials [22,107]. In this case, only the corrective coefficients (α, \dots, μ) were additionally determined through a new fitting, by verifying the conditions reported above, while the regression coefficients (a, \dots, v) determined for fired bricks were maintained also for the equations adopted for stone materials. On the contrary, considering fired bricks materials, the corrective coefficients were set equal to 1, since the model was firstly determined on this type of material.

5.3 Validation of the new failure model

After the fitting operations for the determination of each equation (parameters and scale functions) and their relative significative coefficients, the obtained failure model equation (7) was firstly graphically verified, by overlapping the resulting curves with the average experimental data including their relative standard deviation values.

Then, a quantitative validation was also performed. The confidential R factor [%] was determined for each material and, according to the equation (13). R factor indicates how much the values coming from the failure model differ from the average experimental measurements.

$$R = \sqrt{\frac{\sum_{t=1}^m (X_{fm} - X_{ex})^2}{\sum_{t=1}^m X_{ex}^2}} \cdot 100 \quad (13)$$

In the equation (13), X_{fm} represents the value given by the failure model and X_{ex} the average experimental measurement, respectively at the same time t [19]. A low R value indicated a good agreement between a single curve obtained by the failure model and the related experimental data. According to previous literature works [20–22], an Avrami's curve with a R factor value lower than 25% was considered acceptable.

The validation was performed not only on fired brick materials, but also considering results on stone materials previously investigated [22,107].

Chapter 6

Experimental results

6.1 Results of preliminary algae growth tests under different temperatures

Growth curves of the pure (CM or CF) and mixed (MIX) cultures are reported in Figure 6.1, as the results of the preliminary investigations at different constant temperatures and wet conditions, without the influence of the substrate [95].

Regarding *Chlorella mirabilis* (CM) (Figure 6.1a), an increasing number of cells was counted at both 10 and 27.5 °C. The observed growth trend was in accordance with those reported by Shukla et al. [77], who studied the growth process of *Chlorella mirabilis* in low-temperature environments. The number of the counted cells under $T = 5\text{ °C}$ was constant over the time (attested at about $10^5\text{ cells mL}^{-1}$) and no changes in the growth velocity was observed. On the contrary, at the two higher tested temperatures (35 °C and 40 °C), a remarkable decrease in the cell numbers was noticed, with a considerable reduction of cells after 14 days from the beginning of the tests.

Concerning the growth of *Chroococidiopsis fissurarum* (CF) (Figure 6.1b), no particular effect of the tested temperatures on the growth trend was observed during the overall test, thus confirming the high adaptation capability of cyanobacteria also to the extreme environments [62].

Finally, the growth curves recorded for the mixed cultures (MIX) (Figure 6.1c) substantially reflected the trends of growth curves of the pure cultures. It is noteworthy that the adopted count method of cells did not permit to establish a possible prevalence of a specie over the other one. It is therefore known that, regarding mixed microbial cultures, a competition for nutrients and space can occur, thus leading to a possible prevalence of one species over another [131].

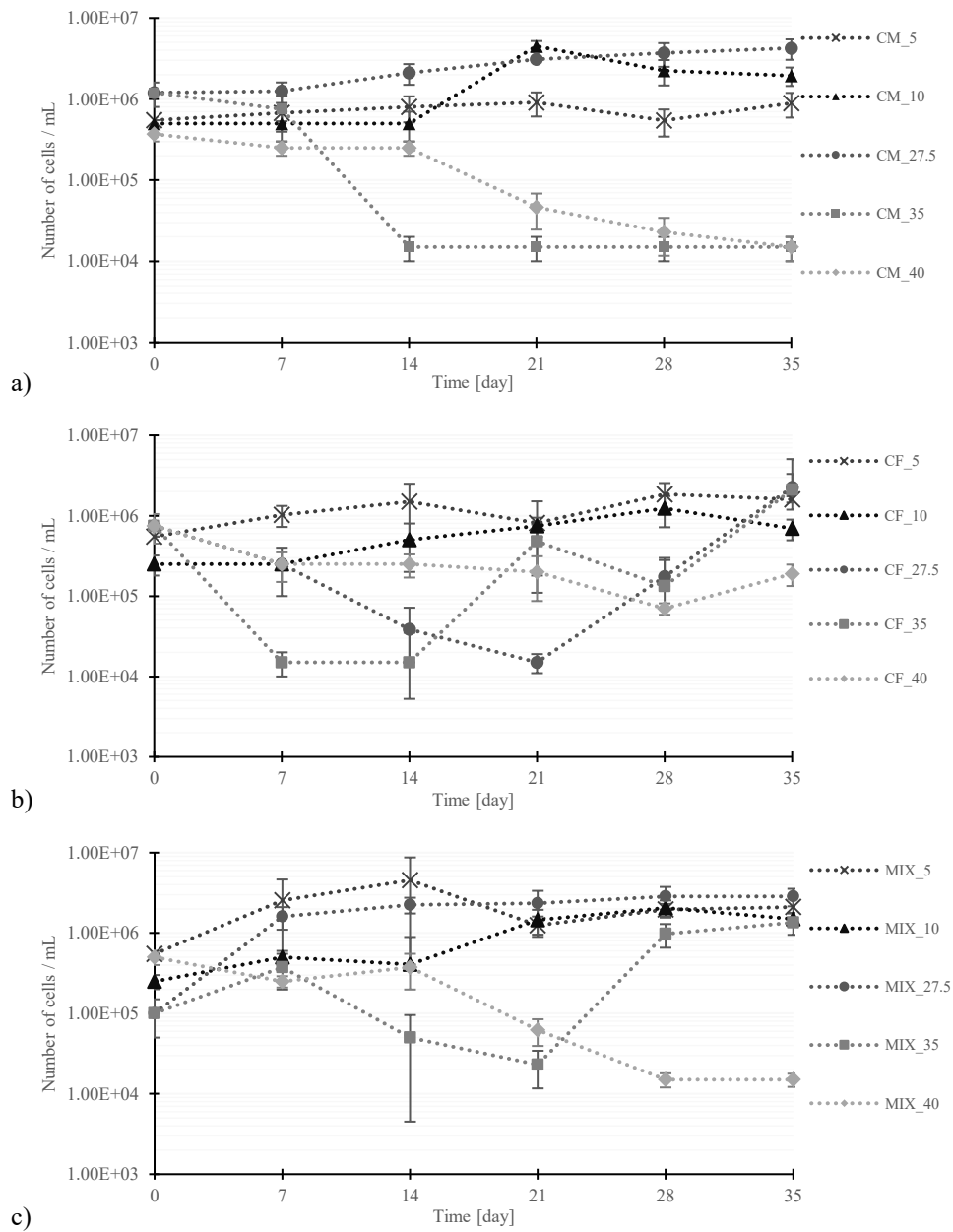


Figure 6.1. Growth curves of: a) *Chlorella mirabilis* CM; b) *Chroococidiopsis fissurarum* CF; c) mixed culture MIX. The growth of the microbial species was tested at five different temperatures.

Considering these preliminary results, the temperatures to set during the following accelerated tests on the fired bricks were selected in order to ensure the presence of both the two colonizing microorganisms. Thus, two different temperatures, $T=10\text{ }^{\circ}\text{C}$ and $T=27.5\text{ }^{\circ}\text{C}$, were chosen as the most suitable temperatures for the growth of both *Chlorella mirabilis* and *Chroococcidiopsis fissurarum*. The selected temperatures correspond to what is reported into the available literature regarding the essential conditions for biological growth on façades [75,76].

6.2 Results of accelerated growth tests under different constant relative humidities

Figure 6.2 (a, b, c) shows the colorimetric analysis carried out by periodically measuring the total colour difference ΔE of the fired brick surfaces exposed to the three different RHs (see Section 4) [95].

Samples B-2R showed no significant differences under the three tested RHs: all the average total colour variations after 36th week were just lower than 1. Samples B-3 showed an average colour variation ΔE even lower than samples B-2R, thus under the limit of human perception. Lastly, average colour variations higher than 1 (but lower than 2) were registered only on samples B-5R from 9th week onward when exposed to $\text{RH}_3 = 98\%$, while an average $\Delta E < 1$ was measured under the other two tested relative humidities (RH_1 and RH_2).

In general, at the end of the 36th week, on most of the samples the average total colour difference ΔE were lower than 1, and only few samples it exceeded this value, but with a chromatic variation noticeable only with a very close observation, since a $\Delta E < 2$ was always observed [125]. On these samples, the red/green difference Δa gave always positive average values (Figure 6.3), thus the hypothesis of a possible chromatic change to green toning due to the presence of chlorophyll was rejected.

In conclusion, it can be assessed that at $\text{RH} \leq 98\%$ no (qualitative) signs of algae growth seemed to be present.

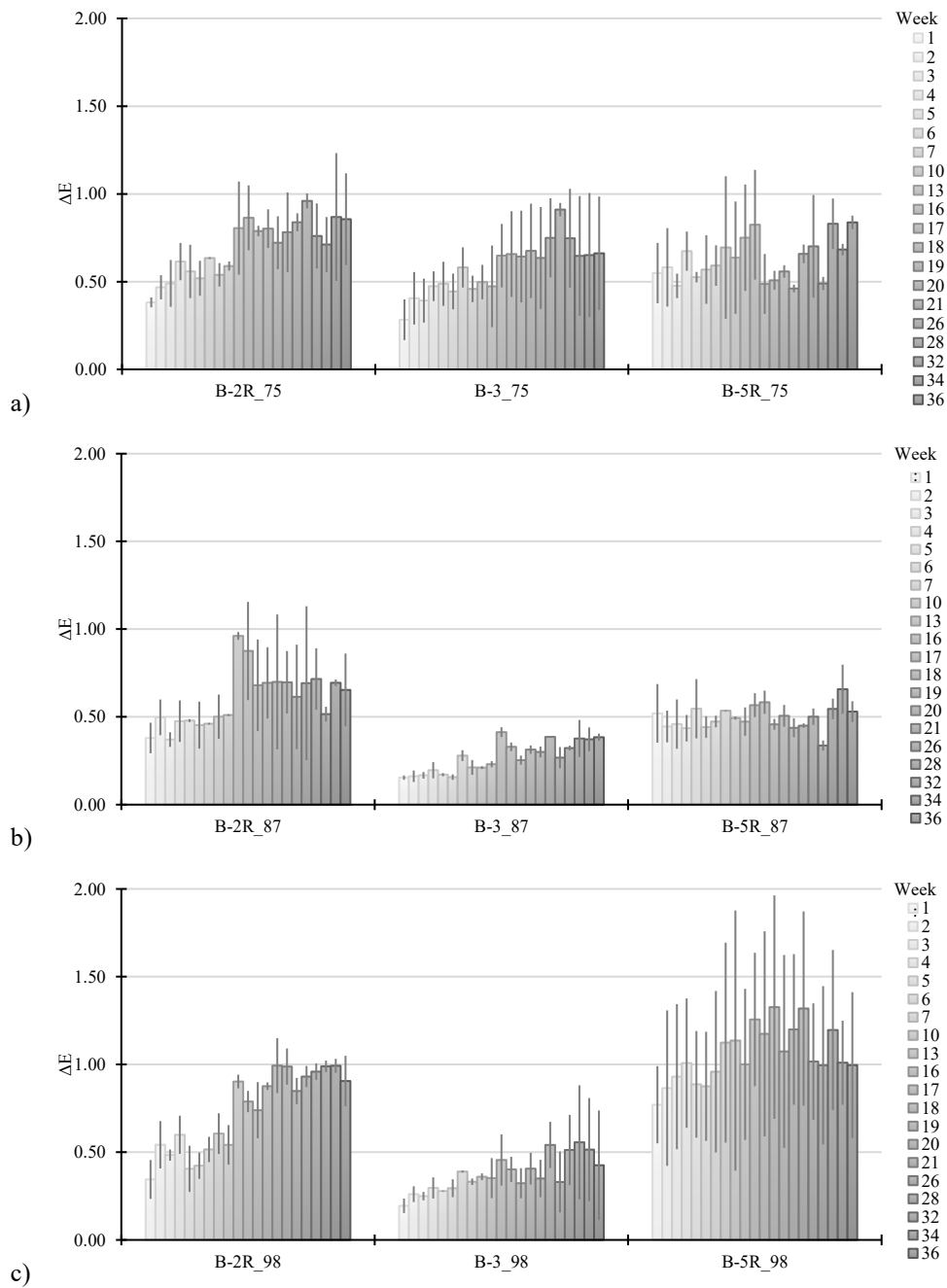


Figure 6.2. Total colour difference ΔE : a) $RH_1=75\%$; b) $RH_2=87\%$; c) $RH_3=98\%$.
Results are reported weekly; vertical line bars indicate standard deviations.

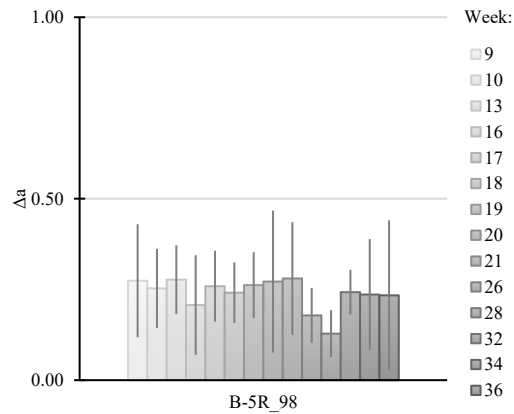


Figure 6.3. Red/green colour difference Δa of sample B-5R_98. Results are reported weekly; vertical line bars indicate standard deviations.

Digital Image Analysis results are shown in Figure 6.4. A synthetic evolution of the surfaces of the B-2, B-3 and B-5 tested sample at the three relative humidity conditions is represented. No differences were detected on the samples before and after the conditioning inside the climatic growth chambers, where they were positioned for 36 weeks [95]. It can be easily seen, also by naked eyes, that the covered area during all the tests under different RHs was always null on each sample.

The results from these scanned images, in term of covered area, quantitatively confirmed the previous qualitative colorimetric analysis: the exposure to $RH \leq 98\%$ does not seem to permit algae to growth on the tested fired bricks' substrates. An eventual presence of algae and cyanobacteria at the microscopic level, not detectable by the instruments used in this work, can also be acceptable since it corresponds to a non-visible algae growth on a façade from an engineering point of view.

| Tested RH _i | Sample | t = 0 week | t = 8 weeks | t = 16 weeks | t = 24 weeks | t = 36 weeks |
|------------------------|--------|------------|-------------|--------------|--------------|--------------|
| RH ₁ (75%) | B-2R | | | | | |
| | B-3 | | | | | |
| | B-5R | | | | | |
| RH ₂ (87%) | B-2R | | | | | |
| | B-3 | | | | | |
| | B-5R | | | | | |
| RH ₃ (98%) | B-2R | | | | | |
| | B-3 | | | | | |
| | B-5R | | | | | |

Figure 6.4. Evolution of the brick samples' surface tested under three different RHs from the beginning (t=0 week) to the end of the test (t=36 weeks).

Conclusively, if RH=98% is assumed as a safety limit to be not overcome, considering the results from both qualitative (colorimetric variation) and quantitative (DIA) evaluations, from an engineering standpoint, it can be assessed that biofouling caused by algae cannot occur on fired brick surfaces at RH<98%. It was also shown that results did not reveal any correlation with the substrate properties, such as total porosity, roughness, and total pore area, but only related to the relative humidity conditions.

6.3 Results of accelerated growth tests under different constant temperatures

The Figure 6.5, Figure 6.6 and Figure 6.7 show the scanned images acquired during the accelerated run-off tests on fired bricks, respectively of smoothed and rough B-2, B-3 and B-5 materials (only one representative sample is here reported for each material). Overall, the experiment at T=10 °C (Test_5) lasted 26 weeks, while the experiment at T=27.5°C (Test_0) lasted 20 weeks. Each material showed different velocities in the biofouling process, and, as a consequence, samples were tested until the stabilization of algal growth was reached.

Generally, the fouling of the samples' surface started with small green spots, and its extension resulted in the proliferation and adhesion of new ones. The simultaneous attachment and growth of the spots as nuclei allows the use of Avrami's model (see Section 3.1).

In addition, the algal spots usually appeared randomly on the samples' surface, and in some cases the biological fouling evolved as streaks due to the suspension flow (sample B-2 and B-5), as commonly observed on deteriorated façades [97].

Concerning the influence of the temperature, it is evident that the samples exposed to T=10 °C were characterized by a reduced fouling respect to the ones exposed to T=27.5 °C.

It is notable, also by naked eye, that rough samples were more covered than the smoothed ones. However, a quantitative analysis of the covered area by algae was needed to investigate more deeply the effect of the substrates' characteristics on the tested bricks, in terms of porosity, roughness and total pore area.











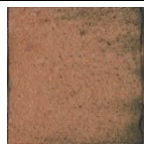



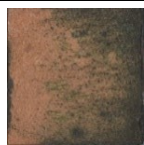


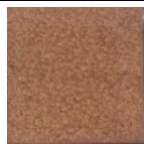
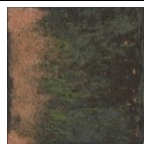
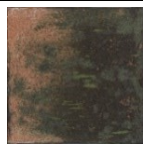


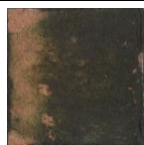
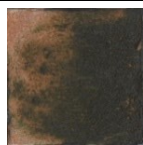
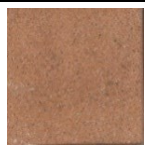

| | | | | |
|--------------|---|---|--|---|
| Tested T_1 | T_1 (10°C) | | T_2 (27.5°C) | |
| Sample | B-2R | B-2S | B-2R | B-2S |
| t = 0 week |  |  |  |  |
| t = 4 weeks |  |  |  |  |
| t = 8 weeks |  |  |  |  |
| t = 12 weeks |  |  |  |  |
| t = 16 weeks |  |  |  |  |
| t = 20 weeks |  |  |  |  |
| t = 24 weeks |  |  | test finished | test finished |

Figure 6.5. Progressive algae coverage on B-2 samples' surfaces during accelerated growth test under different constant temperatures.










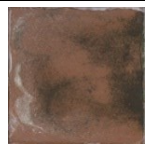

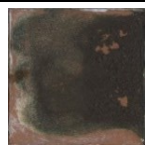
| | | | | | | | |
|-------------------|--------|--|---|--|--|--|--|
| Tested T_i | Sample | t = 0 week | t = 2 weeks | t = 4 weeks | t = 6 weeks | t = 8 weeks | t = 10 weeks |
| T_1 (10°C) | B-3 |  |  |  |  |  |  |
| T_2 (27.5°C) | B-3 |  |  |  |  |  |  |

Figure 6.6. Progressive algae coverage on B-3 samples' surfaces during accelerated growth test under different constant temperatures.




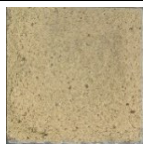
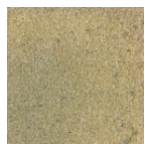
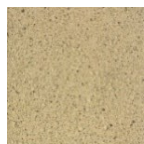


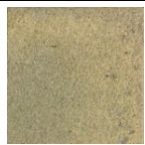
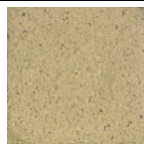
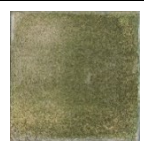






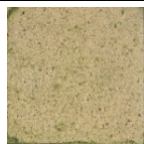




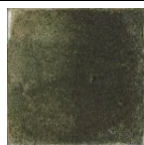



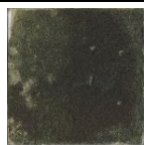

| | | | | |
|--------------|---|---|--|---|
| Tested T_1 | T_1 (10°C) | | T_2 (27.5°C) | |
| Sample | B-5R | B-5S | B-5R | B-5S |
| t = 0 week |  |  |  |  |
| t = 1 week |  |  |  |  |
| t = 2 weeks |  |  |  |  |
| t = 3 weeks |  |  |  |  |
| t = 4 weeks |  |  |  |  |
| t = 5 weeks |  |  |  |  |
| t = 6 weeks |  |  |  |  |

Figure 6.7. Progressive algae coverage on B-5 samples' surfaces during accelerated growth test under different constant temperatures.

Concerning the quantification of the covered area by algae, results obtained by DIA, are reported in Figure 6.8. Graphs show the weekly measurements recorded according to Section 4.6.

After the exposure at $T = 27.5\text{ }^{\circ}\text{C}$, samples B-2R and B-2S showed similar growth processes (Figure 6.8a, b). A very slow growth was registered until 27th day, then the growth rate increased up to the maximum covered area, that in both cases it reached about 80% after 140 days. Considering results from tests at $T=10\text{ }^{\circ}\text{C}$ (Figure 6.8a, b), it is evident how the biofouling process was strongly affected by the lower temperature. Both on B-2R and B-2R, the measured covered area was significantly reduced (less than 10% of the samples' surfaces). At the lower environmental temperature the growth was also delayed. Indeed, the fired bricks were tested for 182 days, that is until the stagnation phase of growth.

A similar behaviour was observed on sample B-3. However, on this type of brick, the samples' surfaces were covered on average only up to 65% of the total area after 63 days at $T=27.5\text{ }^{\circ}\text{C}$, while samples at $T=10^{\circ}\text{C}$ reached on average the 12% of coverage after about 70 days (Figure 6.8c).

Considering samples B-5, both the rough (B-5R) and the smoothed (B-5S) surfaces showed a percentage of covered area equal to 90% when exposed to the temperature of 27.5°C (Figure 6.8d, e). This type of samples reached the higher covered area by algae in the shortest time. Indeed, after 42 days the trend of the registered data reached the stagnation phase. On the contrary at $T=10\text{ }^{\circ}\text{C}$ (Figure 6.8d, e), B-5R and B-5S samples showed on average the maximum algal coverage only for the 35% of the total area after 49 days.

Looking at all the graphs, it can be noticed that the higher is the porosity of the substrate, the shorter is the time for a complete biofouling, that is until the stagnation phase.

Moreover, comparing the measurements of the two accelerated tests, it is possible to assess that the covered area decreased when the samples were exposed to a colder temperature ($T=10^{\circ}\text{C}$). Moreover, the lower temperature extended the growth process time by 15%÷30%.

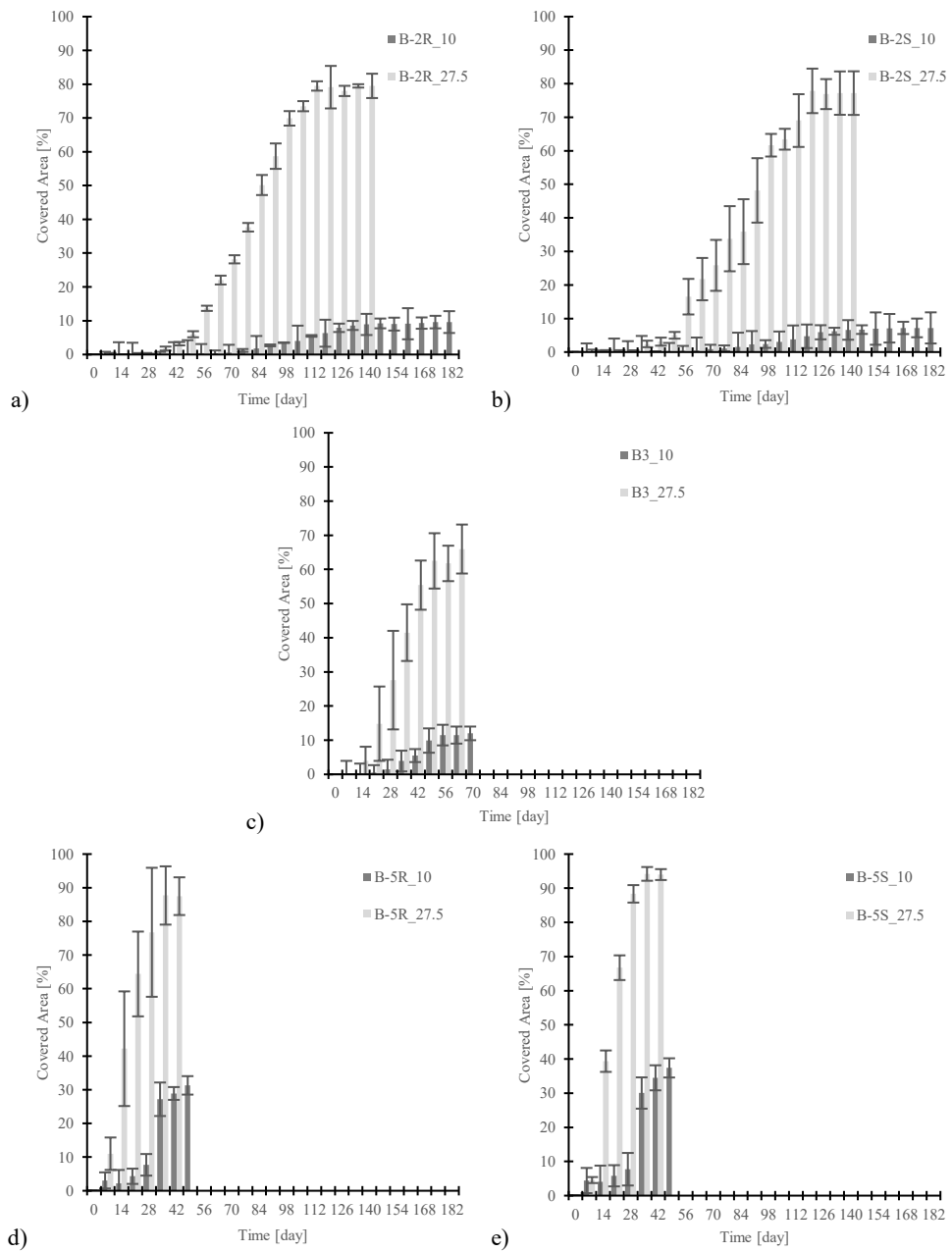


Figure 6.8. Average area coverage area of fired bricks: a) samples B-2R; b) samples B-2S; c) samples B-3; d) samples B-5R; e) samples B-5S. Results for $T=10^{\circ}\text{C}$ are displayed in black, while results for $T=27.5^{\circ}\text{C}$ in grey. Vertical lines indicate standard deviations.

6.4 The influence of substrate properties on algae growth under constant temperatures

Figure 6.9a reports the number of days until the stagnation phase was reached on each sample. No significant differences were noticed between rough and smoothed samples. However, it is evident how a high porous brick, as samples B-5 (44.09%, Table 4.4), accelerated the biofouling process in terms of time, if compared to a low porous brick, as samples B-2 (19.24%, Table 4.4). Porosity also influenced the effect of temperature. The duration of the biofouling process on high porous samples (B-5) was increased by 15% when exposed at a colder temperature ($T=10\text{ }^{\circ}\text{C}$). On the contrary, for the less porous substrate (samples B-2) the time process was increased by 30%. Thus, the effect of temperature was enhanced on sample characterized by low porosity.

The effect of roughness on the average covered area at the end of the tests is reported in Figure 6.9b. The higher roughness values of samples B-5S and B-5R ($6.60\text{ }\mu\text{m}$ and $7.60\text{ }\mu\text{m}$, Table 4.4) favoured the algae growth, if compared to sample B-3, characterized by a lower roughness ($2.95\text{ }\mu\text{m}$, Table 4.4). Roughness influenced the effect of temperature, too. On sample B-5 the average algal coverage decreased by 60%, while on low rough samples (B-3) it was decreased by 80%.

Regarding the total pore area, no clear correlations were found, considering the covered area at the end of the tests and the time to reach the maximum biofouling on brick samples (Figure 6.9c-d). However, since the total pore area is a property linked to the pore structure [118,132,133], it could influence the behaviour of the material regarding the storage of water inside the material pores.

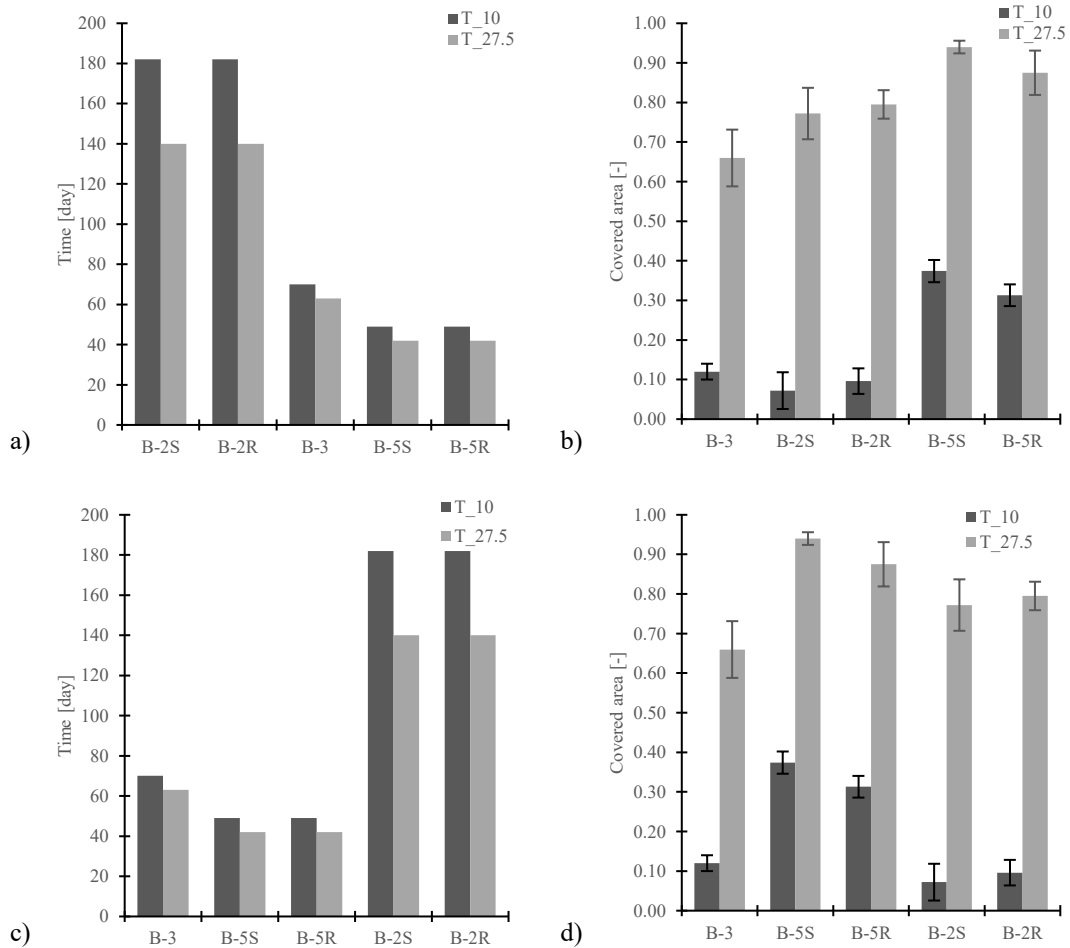


Figure 6.9. a) Duration of the accelerated biofouling process on tested fired bricks in ascending order of porosity; b) Average covered area by algae at the end of the tests on tested bricks in ascending order of roughness; c) Time needed for a complete biofouling process on samples in ascending order of total pore area; d) Final average covered area on samples in ascending order of total pore area.

Finally, it can be pointed out that porosity mainly influenced the rate of biofouling process: a higher value of porosity corresponded to a faster algae growth. At the same time, roughness mainly affected the covered area reached at the end of the biofouling: the percentage of algal coverage had an increasing trend from smoother to rougher surfaces.

SEM investigations on fired bricks were performed on B-2R and B-5R samples, collected after accelerated growth tests under optimal growth conditions (27.5 ± 2.5 °C), in order to take into account the lowest and highest porosity and different roughness. In Figure 6.10 the SEM micrographs show the presence of tested algae and cyanobacteria on the two tested fired brick surfaces.

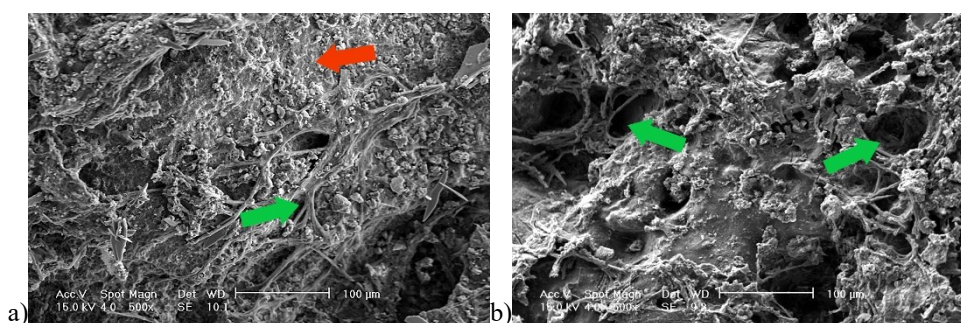


Figure 6.10. SEM micrographs (magnification 500x) of B-2R and B-5R samples collected at the end of the accelerated growth test. a) On B-2R sample, algae and cyanobacteria (green arrow) grown close to the pores, taking advantage of the micro-asperities of the substrate but leaving free the smoother surface (red arrow); b) On B-5R sample, algae and cyanobacteria grown inside pore cavities (green arrows) and adhered to the many irregularities of the surface.

It is evident that the biofouling was represented by filaments, that were gathered mainly along and across the pore micro-cavities and clung to the micro-asperities of the rough surface of the substrates. Thus, it is reasonable to suppose that the presence of pores facilitates the settlement of the biofouling, while an irregular surface (roughness) its spread.

This assumption seems to confirm what previously deduced from Figure 6.9. In other words, on the one side, the lower the porosity the higher the stagnation time, because the biofouling needs time to link together from one pore to another. On the other side, the higher the roughness the higher the covered area, because the presence of micro-indentations on the material surface favours the mechanical anchorage of the microbial cells, which progressively proliferated and grew, forming filamentous algal biomass. Clearly, a high porosity joined to a high roughness causes low stagnation times, as well as a great spread of the biofouling, that is a high covered area.

Chapter 7

Modelling of the experimental results

7.1 Effect of temperature modelled with the previous Avrami's model

According to the modified Avrami's equation (1), growth curves $X(t)$ were analytically modelled with the parameters obtained from the accelerated growth tests at $T=27.5$ °C and $T=10$ °C. Results are reported in Figure 7.1. The graphs show the results about the materials experimentally tested in this research (samples B-2, B-3 and B-5), while the results of the other fired brick materials (B-1 and B-4) can be found in literature [21].

The experimental measurements of the covered area for each material are displayed as vertical bars, reported as standard deviations of the measurements weekly acquired on three samples.

These results confirmed the experimental findings, also reported in Figure 6.8. The effect of the temperature is well represented, since the curves associated to the lower temperature were clearly lower in terms of covered area and delayed in time respect to the curves related to the optimal temperature.

For all the samples, the curves on average tended to slightly underestimate the initial part of experimental results and, on the contrary, to slightly overestimate the growth process in the proximity of the last stagnation phase. However, since the analytical values were generally included within the standard deviations of the average experimental values, it can be assessed that the analytical curves, obtained with the modified Avrami's equation (1), well modelled the experimental measurements, both for the optimal and the non-optimal tested temperatures.

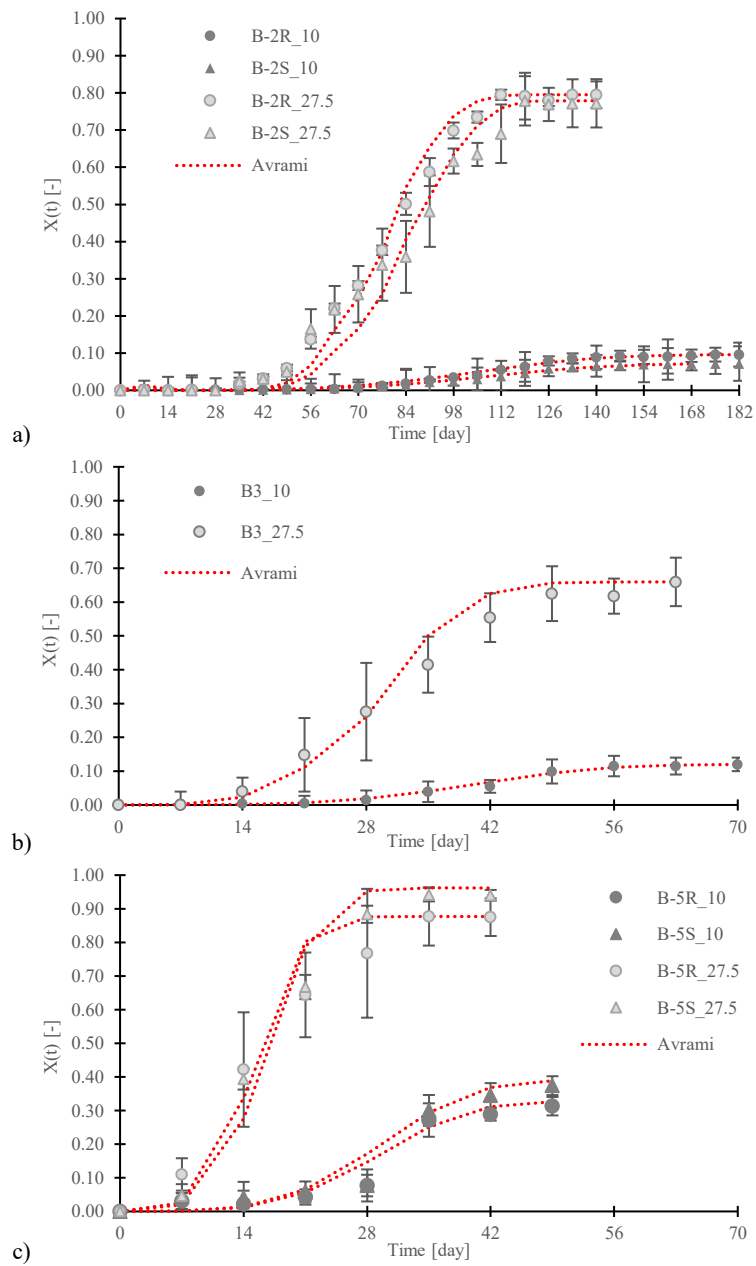


Figure 7.1. Overlapping of the Avrami's curves to experimental data: a) B-2R and AS samples; b) B-3 sample; c) B-5R and B-5S sample. Results for $T=10^\circ\text{C}$ are reported in black, results for $T=27.5^\circ\text{C}$ are reported in grey, red dotted lines indicate Avrami's curves. Vertical lines indicate standard deviations.

Table 7.1 shows the parameters calculated from the experimental measurements (see Section 5.1.1) and used for the analytical calculation of $\bar{X}(t)$, according to the modified Avrami's equation (1).

Concerning the accelerated growth tests at temperature of 27.5 °C, the final covered area ratio A_c/A_t ranged on average from 66% for samples B-3, to the maximum of 94.2% for samples B-5S. K values were significantly different from each other, and they ranged from $7.00 \cdot 10^{-8}$ for samples B-2S to $1.27 \cdot 10^{-5}$ for samples B-5R. Only on B-2 surfaces, of both rough and smoothed samples, a latency time t_l was observed and it was equal to 27 days.

On the contrary, considering the parameters calculated after the tests at the temperature of 10 °C, the maximum covered area A_c/A_t reached only the 35.2% on samples B-5S (about three times lower than in the case of optimal temperature). K values ranged from $9.74 \cdot 10^{-7}$ for samples B-5S to $5.32 \cdot 10^{-9}$ for samples B-2S. Latency time t_l was found the same as for temperature of 27.5 °C (equal to about 27 days for B-2 samples, and almost null for the other samples).

Generally, after the tests at lower temperature, values of the parameters A_c/A_t and K had a severe decrease: except for samples B-3, growth rate K diminished more than 10 times and A_c/A_t was reduced up to 35%. On the contrary, temperature seemed not to have effect on the latency time t_l .

| Sample | Temperature tested [°C] | A_c/A_t [-] | K [-] | t_l [day] | R [%] |
|--------|-------------------------|---------------|----------------------|-------------|---------|
| B-2R | 27.5 | 0.795 | $1.10 \cdot 10^{-7}$ | 27 | 5 |
| B-2S | | 0.779 | $7.00 \cdot 10^{-8}$ | 27 | 10 |
| B-3 | | 0.660 | $9.47 \cdot 10^{-7}$ | 0 | 9 |
| B-5R | | 0.877 | $1.27 \cdot 10^{-5}$ | 0 | 10 |
| B-5S | | 0.942 | $8.80 \cdot 10^{-6}$ | 0 | 8 |
| B-2R | 10 | 0.096 | $5.94 \cdot 10^{-9}$ | 27 | 7 |
| B-2S | | 0.072 | $5.32 \cdot 10^{-9}$ | 27 | 4 |
| B-3 | | 0.120 | $2.68 \cdot 10^{-7}$ | 0 | 7 |
| B-5R | | 0.327 | $9.74 \cdot 10^{-7}$ | 0 | 12 |
| B-5S | | 0.352 | $9.40 \cdot 10^{-7}$ | 0 | 12 |

Table 7.1. Avrami's parameters determined after the accelerated tests at constant temperature on fired bricks.

Finally, in Table 7.1 the R factor values for each material are reported, to indicate in percentage how much the analytical curves differed from the data experimentally obtained. Values ranged between 5% and 10% for the optimal temperature ($T=27.5$ °C) and between 4% and 12% for the colder tested temperature ($T=10$ °C). Thus, it can be reasonably stated that the modified Avrami's law (equation (1)) is adequate to describe algal growth also for temperatures lower than the optimal one.

7.2 Results about the scaling effect of environmental conditions

Table 7.2 shows the effect of relative humidity on algal growth for each tested sample. The Ω values, determined according to equation (11), were equal to 0 for all the performed RH tests. In these cases indeed, in spite of the high level of relative humidity maintained inside the growth chambers, the environmental conditions did not provide on the samples' surface free water to assure biological activity. According to the adopted calculation method (see Section 5.1.2), the Ω value was equal to 1, only in presence of water streaming on the samples' surface, such as in Test_0 with wet&dry cycles ($RH \geq 98\%$).

| RH condition | Ω value |
|---|----------------|
| Test_0: $RH \geq 98\%$, wet&dry cycles | 1 |
| Test_1: $75 \pm 2\%$ RH | 0 |
| Test_2: $87 \pm 2\%$ RH | 0 |
| Test_3: $98 \pm 2\%$ RH | 0 |

Table 7.2. Ω values determined from experimental results under tested relative humidities.

Concerning the scale functions τ_i , used to take into account the effect of temperature on the biofouling process, Table 7.3 lists the τ_A and τ_K values (related to A_o/A_f and K parameters), calculated for each fired brick tested at $T=10$ °C (Test_5) according to the equation (12). Since for all the tested samples under $T=10$ °C, the latency time t_l showed no differences if compare to experiments at $T=27.5$ °C, the scale values τ_{t1} were considered equal to 1.

No significant growth was detected during the preliminary tests on temperatures $T=5$ °C and $T=40$ °C (Test_4 and Test_6), thus τ_A and τ_K were assumed null; on the contrary, τ_{t1} was assumed tending towards an infinite value. Adopting these values for the scale functions in equation (7), the absence of growth can be well simulated.

Moreover, having assumed $T=27.5$ °C as the reference value, all the τ_i scale functions were equal to 1 in case of temperature $T = 27.5$ °C.

| Sample | τ_A | τ_K |
|--------|----------|----------|
| B-2S | 0.12 | 0.09 |
| B-2R | 0.10 | 0.10 |
| B-3 | 0.19 | 0.11 |
| B-5S | 0.35 | 0.15 |
| B-5R | 0.33 | 0.15 |

Table 7.3. Experimental results for τ_A and τ_K of Test_5 ($T=10$ °C).

7.3 Equations of the implemented Avrami's parameters based on fired bricks

According to the method described in Section 5.2.2, the experimental results of the Tests_0 (tests performed at T= 27.5 °C) were fitted with the substrate properties of the tested fired bricks, in order to express the A_c/A_t , K and t_l parameters as functions of the substrate properties (P , A and R). The resulting equations of the parameters A_c/A_t , K and t_l are listed in (14)-(16).

$$\frac{A_c}{A_t}(P, R, A) = 1 - e^{-\alpha \cdot (a \cdot P + b \cdot R + c \cdot A + d)^4} \quad (14)$$

$$K(P, R, A) = 1 - e^{-\beta \cdot \left(\frac{g \cdot P + h \cdot R + i \cdot A + j}{l} \right)^2} \quad (15)$$

$$t_l(P, R, A) = \gamma \cdot \frac{m}{(n \cdot P + o \cdot R + p \cdot A + q)^2} \quad (16)$$

The equations for the final covered area ratio A_c/A_t and rate parameter K showed an increase trend with the variables (P , A and R), while the latency time t_l had an inverse trend. Table 7.4 shows the significant variables and the respective numerical values of the regression coefficients for the three parameters the A_c/A_t , K and t_l .

For the A_c/A_t parameter, in equation (14), the resulted significant variables were porosity P and roughness R , respectively multiplied by the regression coefficients a and b . The regression coefficient c of the total pore area A and the constant term d were about zero, thus they were not taken into account. Regarding to the K parameter of equation (15), the variables with significant regression coefficients (g , i) were found to be porosity P and total area A , both with the same regression coefficient value. Finally, the latency time t_l in equation (16) was found to be only a function of roughness R , and its regression coefficient o was equal to 1.

| Parameter | P | R | A | Constant term |
|-----------|--------------------------|-------------|--------------------------|--|
| A_c/A_t | $a = 2.480$ | $b = 0.126$ | $c = 0$ | $d = 0$ |
| K | $g = 4.49 \cdot 10^{-3}$ | $h = 0$ | $i = 4.49 \cdot 10^{-3}$ | $j = 5.79 \cdot 10^{-3}$, $l = 2.09$ |
| t_l | $n = 0$ | $o = 1$ | $p = 0$ | $m = 5$, $q = -5.02$ |

Table 7.4. Avrami's parameters for fired brick materials: regression coefficients associated to the substrate variables (porosity P , roughness R and total pore area A).

Concerning the corrective coefficients (α , β and γ), provided into the model to take into account the eventual secondary effects on growth related to the nature of different materials, in the case of the fired bricks considered in this Section they were assumed equal to 1, since the model was firstly determined on this type of material.

Finally, the resulting functions of A_c/A_t , K and t_l parameter for fired brick materials, with only the significative variables, are reported in equations (17)-(19).

$$\frac{A_c}{A_t}(P, R) = 1 - e^{-(2.48 \cdot P + 0.126 \cdot R)^4} \quad (17)$$

$$K(P, A) = 1 - e^{-\left(\frac{4.49 \cdot 10^{-3} \cdot P + 4.49 \cdot 10^{-3} \cdot A + 5.79 \cdot 10^{-3}}{2.09}\right)^2} \quad (18)$$

$$t_l(R) = \frac{5}{(R - 5.02)^2} \quad (19)$$

An acceptable agreement between values of the parameters experimentally determined (according to Section 5.1.1) and the values obtained with the above equations (17)-(19), was obtained. The coefficients of determination R^2 are reported in figure (Figure 7.2).

The parameter A_c/A_t of equation (14) showed a very good correlation with the experimental data, with a $R^2=0.91$ (Figure 7.2a). The growth rate K in equation (15) exhibited not a high correlation factor ($R^2=0.76$, Figure 7.2), but equation (18) was able to well simulate the growth rate calculated with the implemented failure model (equation (7)) according to the experimental findings. Finally and the latency time equation (16) had $R^2=0.99$ (Figure 7.2c).

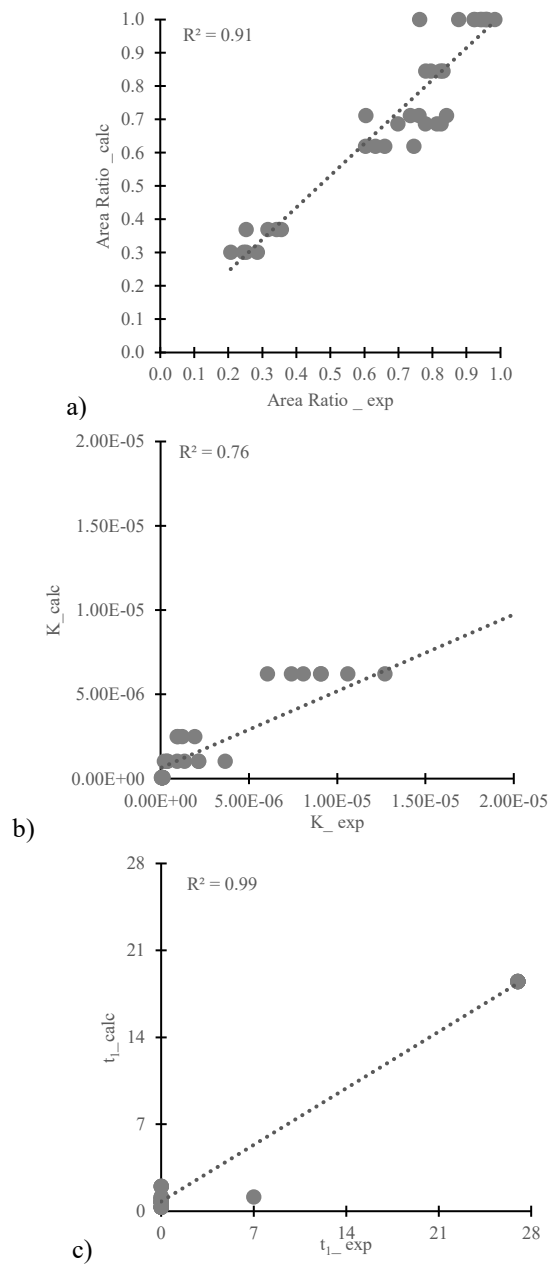


Figure 7.2. Correlation between experimental and calculated Avrami's parameters for fired brick materials: a) final covered area ratio A_c/A_t , b) growth rate K , and c) latency time t_l .

7.4 Equations of the scale functions of environmental conditions based on fired bricks

Based on to the experimental results (Table 7.2), the Ω scale function had a binary trend in accordance with high levels of RH and free water availability, while it was not related to the substrate properties. Hence, the equation (20) shows the formula implemented in the failure model.

$$\Omega = f(RH) = \begin{cases} 0, & RH < 98\% \\ 1, & RH \geq 98\% \end{cases} \quad (20)$$

According to this set, Ω parameter was equal to 1 only when relative humidity was at least equal to 98% and in presence of water on the material surface. For other cases, Ω was set to 0, nullifying the result of equation (7). From a more precautionary engineering standpoint, the Ω scale function was assumed equal to 1 also for relative humidity values equal or higher than 98%, instead of considering only free water availability.

Also the scale function of temperature on the latency time τ_{t1} was directly determined from experimental data (Table 7.3), thus it was not subjected to fitting. The equation (21) shows the resulting temperature scale function τ_{t1} for the latency time t_l :

$$\begin{cases} \tau_{t1}(T) \approx 1, & 5^\circ\text{C} < T < 10^\circ\text{C} \\ \tau_{t1}(T) = 1, & 10^\circ\text{C} \leq T \leq 27.5^\circ\text{C} \\ \tau_{t1}(T) \approx 1, & 27.5^\circ\text{C} < T < 40^\circ\text{C} \end{cases} \quad (21)$$

where, in accordance with the experimental results (see Section 7.2), the scale function can be stated equal to 1 for a temperature ranging between 10°C and 27.5°C . For the other ranges, τ_{t1} was assumed equal to 1, but future works should investigate other temperatures, in order to validate or confute this hypothesis.

The formulations of the parameters τ_A and τ_K are shown in the equations (22) and (23). Both equations were cubical functions of temperature. The coefficients of determination R^2 showed a perfect agreement between experimental and calculated values: (both R^2 were equal to 1).

$$\tau_A(T) = r_A \cdot T^3 + s_A \cdot T^2 + u_A \cdot T + v_A \quad (22)$$

$$\tau_K(T) = r_K \cdot T^3 + s_K \cdot T^2 + u_K \cdot T + v_K \quad (23)$$

The regression coefficients r , s , u and v , respectively for τ_A and τ_K are presented in the equations (24) and (25). Since both the scale functions τ_A and τ_K experimentally determined (in Table 7.3) showed a correlation with the substrate properties (P , R , A), the regression coefficients (a^I , b^I , ..., d^{IV}) were determined.

$$\begin{cases} r_A(P, R, A) = \delta_A (a^I \cdot P + b^I \cdot R + c^I \cdot A + d^I) \\ s_A(P, R, A) = \eta_A (a^{II} \cdot P + b^{II} \cdot R + c^{II} \cdot A + d^{II}) \\ u_A(P, R, A) = \lambda_A (a^{III} \cdot P + b^{III} \cdot R + c^{III} \cdot A + d^{III}) \\ v_A(P, R, A) = \mu_A (a^{IV} \cdot P + b^{IV} \cdot R + c^{IV} \cdot A + d^{IV}) \end{cases} \quad (24)$$

$$\begin{cases} r_K(P, R, A) = \delta_K (a^I \cdot P + b^I \cdot R + c^I \cdot A + d^I) \\ s_K(P, R, A) = \eta_K (a^{II} \cdot P + b^{II} \cdot R + c^{II} \cdot A + d^{II}) \\ u_K(P, R, A) = \lambda_K (a^{III} \cdot P + b^{III} \cdot R + c^{III} \cdot A + d^{III}) \\ v_K(P, R, A) = \mu_K (a^{IV} \cdot P + b^{IV} \cdot R + c^{IV} \cdot A + d^{IV}) \end{cases} \quad (25)$$

Table 7.5 shows that, as a result of the fitting process, all the equations of the sets (24) and (25) are only functions of porosity P and roughness R . Since the regression coefficient c^i did not assumed any significant value, it was simply considered equal to zero. In general, all the regression coefficients of the τ_A and τ_K scale functions, respectively r_A , s_A , u_A , v_A and r_K , s_K , u_K , v_K in equations (22) and (23), resulted significant.

| Regression coefficient | P | R | A | Constant term |
|------------------------|----------------------------------|-----------------------------------|---------------|-----------------------------------|
| r_A | $a^I = 3.8447 \cdot 10^{-4}$ | $b^I = -4.0800 \cdot 10^{-6}$ | $c^I = 0$ | $d^I = -2.1164 \cdot 10^{-4}$ |
| s_A | $a^{II} = -2.7874 \cdot 10^{-2}$ | $b^{II} = 2.9590 \cdot 10^{-4}$ | $c^{II} = 0$ | $d^{II} = 1.1856 \cdot 10^{-2}$ |
| u_A | $a^{III} = 5.5270 \cdot 10^{-1}$ | $b^{III} = -5.8670 \cdot 10^{-3}$ | $c^{III} = 0$ | $d^{III} = -1.4727 \cdot 10^{-1}$ |
| v_A | $a^{IV} = -2.1146$ | $b^{IV} = 2.2450 \cdot 10^{-2}$ | $c^{IV} = 0$ | $d^{IV} = 4.7041 \cdot 10^{-1}$ |
| r_K | $a^I = 8.3270 \cdot 10^{-5}$ | $b^I = 6.7000 \cdot 10^{-7}$ | $c^I = 0$ | $d^I = -1.8459 \cdot 10^{-4}$ |
| s_K | $a^{II} = -6.0378 \cdot 10^{-3}$ | $b^{II} = -4.8800 \cdot 10^{-5}$ | $c^{II} = 0$ | $d^{II} = 9.8770 \cdot 10^{-3}$ |
| u_K | $a^{III} = 1.1971 \cdot 10^{-1}$ | $b^{III} = 9.6900 \cdot 10^{-4}$ | $c^{III} = 0$ | $d^{III} = -1.0759 \cdot 10^{-1}$ |
| v_K | $a^{IV} = -4.5803 \cdot 10^{-1}$ | $b^{IV} = -3.7100 \cdot 10^{-3}$ | $c^{IV} = 0$ | $d^{IV} = 3.1809 \cdot 10^{-1}$ |

Table 7.5. Regression coefficients determined for the substrate variables (P , R , A) of the temperature scale functions τ_A and τ_K .

Figure 7.3a and Figure 7.3b show the trend of the functions τ_A and τ_K , respectively scaling the parameters A_o/A_t and K , in the range between 5°C and 40°C. Both τ_A and τ_K functions reach the maximum value in the temperatures comprised between 25°C and 30°C, hence inside the optimal range of growth for the tested algae [71,73].

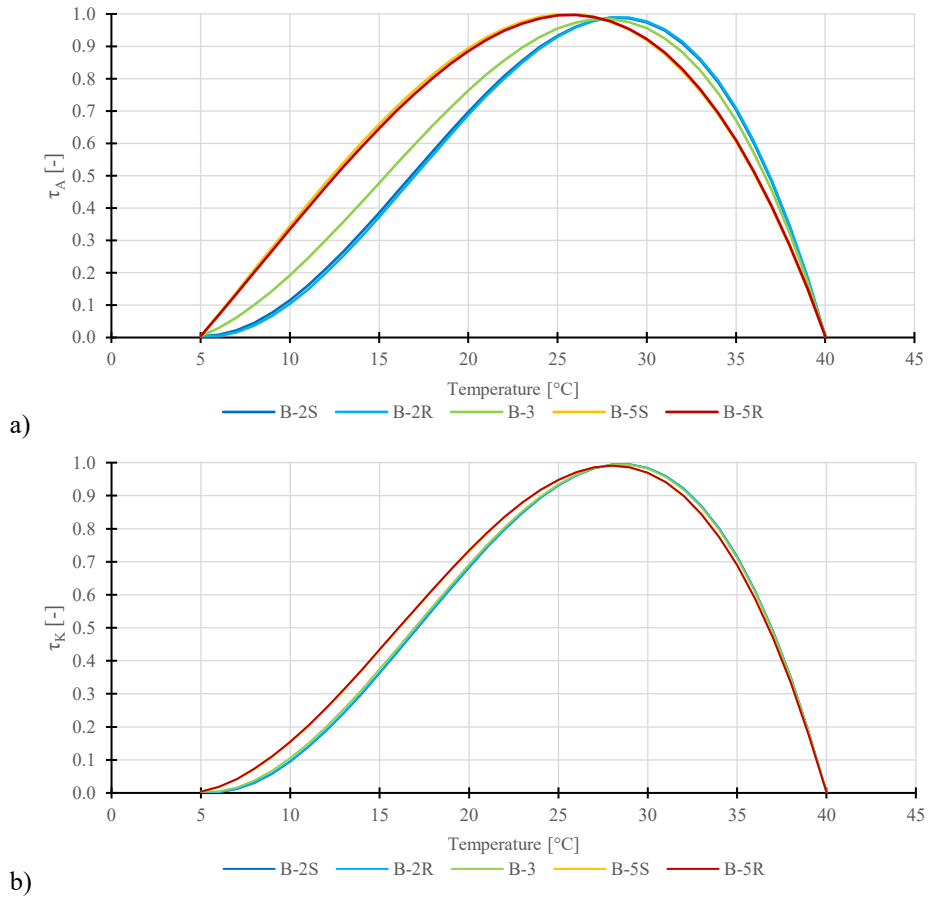


Figure 7.3. Trend of the scale functions a) τ_A and b) τ_K for the tested fired brick materials.

Using the data of Table 7.3, both the equations (22) and (23) showed a coefficients of determination R^2 equal to 0.99, hence a perfect agreement between experimental and calculated values was found.

7.5 Corrective coefficients for stone materials

According to the results of a previous work [22], by fitting the experimental data about stones, it was possible to determine the corrective coefficients for stone materials (α , β and γ). In this way the regression coefficients determined for the A_c/A_t , K and t_l parameter of fired bricks remained valid and adequate also for stone substrates. Moreover, all the three conditions imposed for the iterative fitting process (see Section 5.2.2) were respected. The corrective coefficients (α , β and γ) of the failure models' parameters A_c/A_t , K and t_l for stones, expressed in equations (14)-(16), are shown in Table 7.6.

| Parameter | Corrective coefficient | |
|-----------|------------------------|------------|
| A_c/A_t | $\alpha = 2$ | sandstones |
| | $\alpha = 100$ | limestones |
| K | $\beta = 1.724$ | sandstones |
| | $\beta = 6.897$ | limestones |
| t_l | $\gamma = 0.2$ | sandstones |
| | $\gamma = 1.6$ | limestones |

Table 7.6. Calculated values of corrective coefficients for sandstone and limestone materials.

These coefficients have been determined for sandstone and limestone substrates [22], but according to Section 5.2.2 this process could be applied on further different substrates in order to extend the model to others building materials.

7.6 Validation of the failure model

In this Section, Figure 7.4, Figure 7.5 and Figure 7.6 present the growth curves obtained by the new failure model compared to the experimental data about fired bricks materials. As expected, the typical sigmoidal curve was returned, representing the typical biofouling process over time on building materials [19].

The model was able to simulate the biodeterioration observed during the tests performed under optimal environmental conditions for growth, at $T=27.5^{\circ}\text{C}$, $\text{RH} \geq 98\%$ and with “wet&dry” cycles (Figure 7.4 and Figure 7.5)

In particular the different evolutions of covered area on the samples' surfaces was well reproduced by the model, according to the different substrate properties of the fired bricks. Also the velocities of the different biofouling processes were simulated. Indeed, the faster biodegradation of the most porous materials, respect to the less porous, was rightly represented, as well as the final covered area, according to the different surface roughness of the substrates.

Figure 7.5 show the growth curves obtained by the failure model about the materials tested in Graziani et al. [21]. The model slightly overestimated the final covered area of B1-R and B-1S samples, and the overall growth rate of the B-4S sample, but, since this material reached a final covered area of almost 100%, it can be acceptable from a precautionary engineering point of view.

Finally, Figure 7.6 reports the failure model curves for the materials tested under the environmental condition of Test_5 ($T=10^{\circ}\text{C}$; $\text{RH} \geq 98\%$ and “wet&dry” cycles). In this case, the low temperature strongly reduced the covered area during the process, limiting the degradation of the materials. Also for this environmental condition, the growth curves, properly decreased by τ_i values, were close to the experimental data, and a good reproducibility of the measurements was obtained.

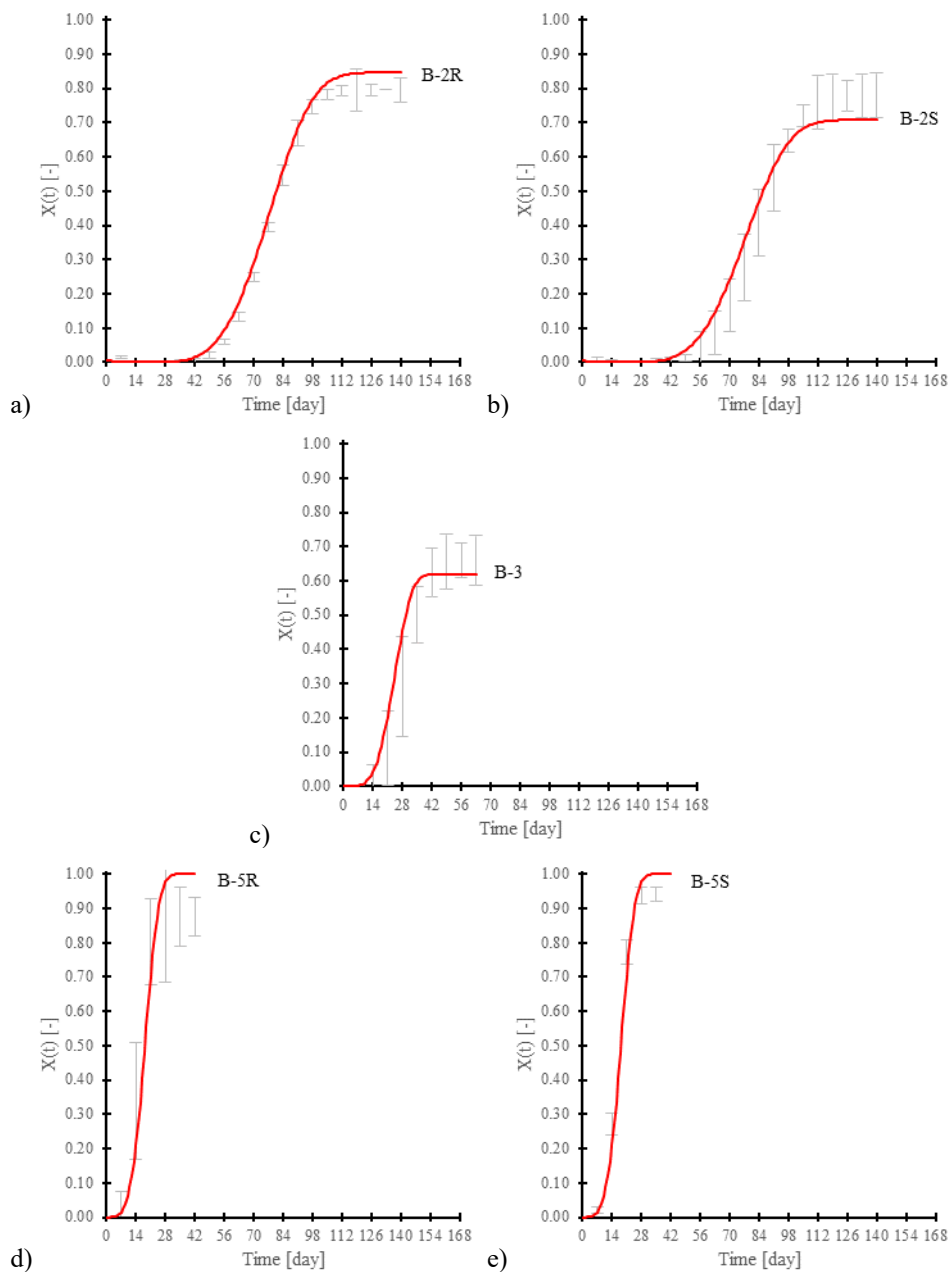


Figure 7.4. Growth curves, calculated with the implemented failure model, on the fired brick materials tested in this research under optimal environmental conditions (Test_0). Vertical lines indicate the standard errors of experimental measurements.

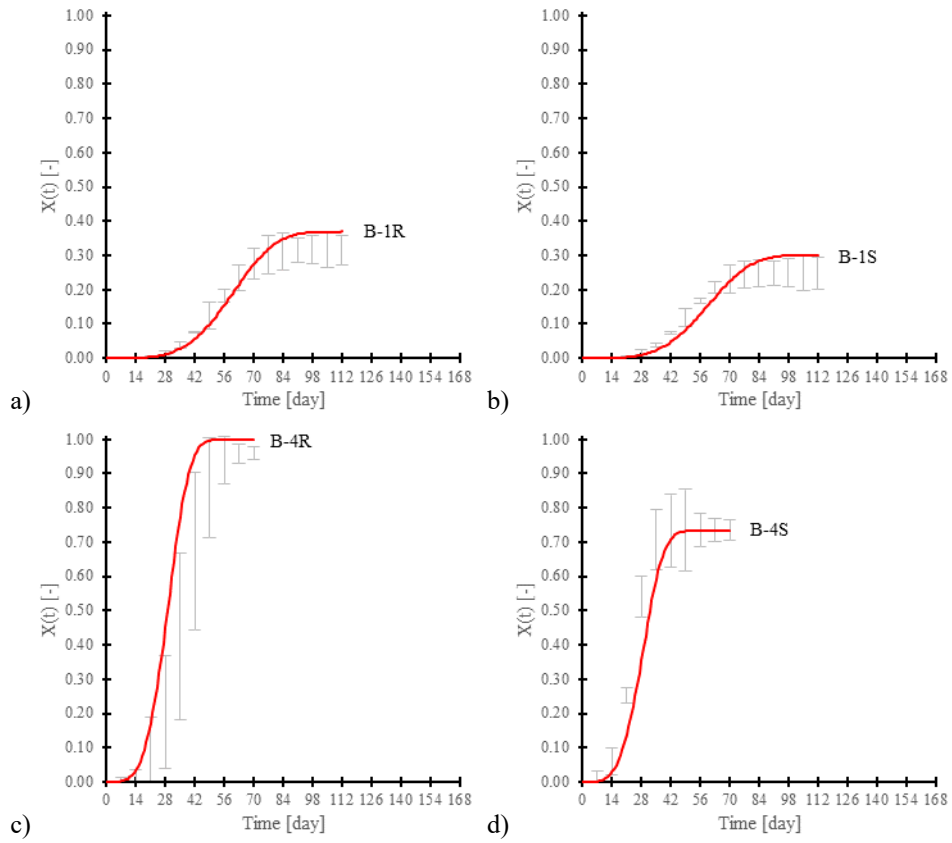


Figure 7.5. Growth curves, calculated with the implemented failure model, on the fired brick materials tested in Graziani et al. [21] under optimal environmental conditions (Test_0). Vertical lines indicate the standard errors of experimental measurements.

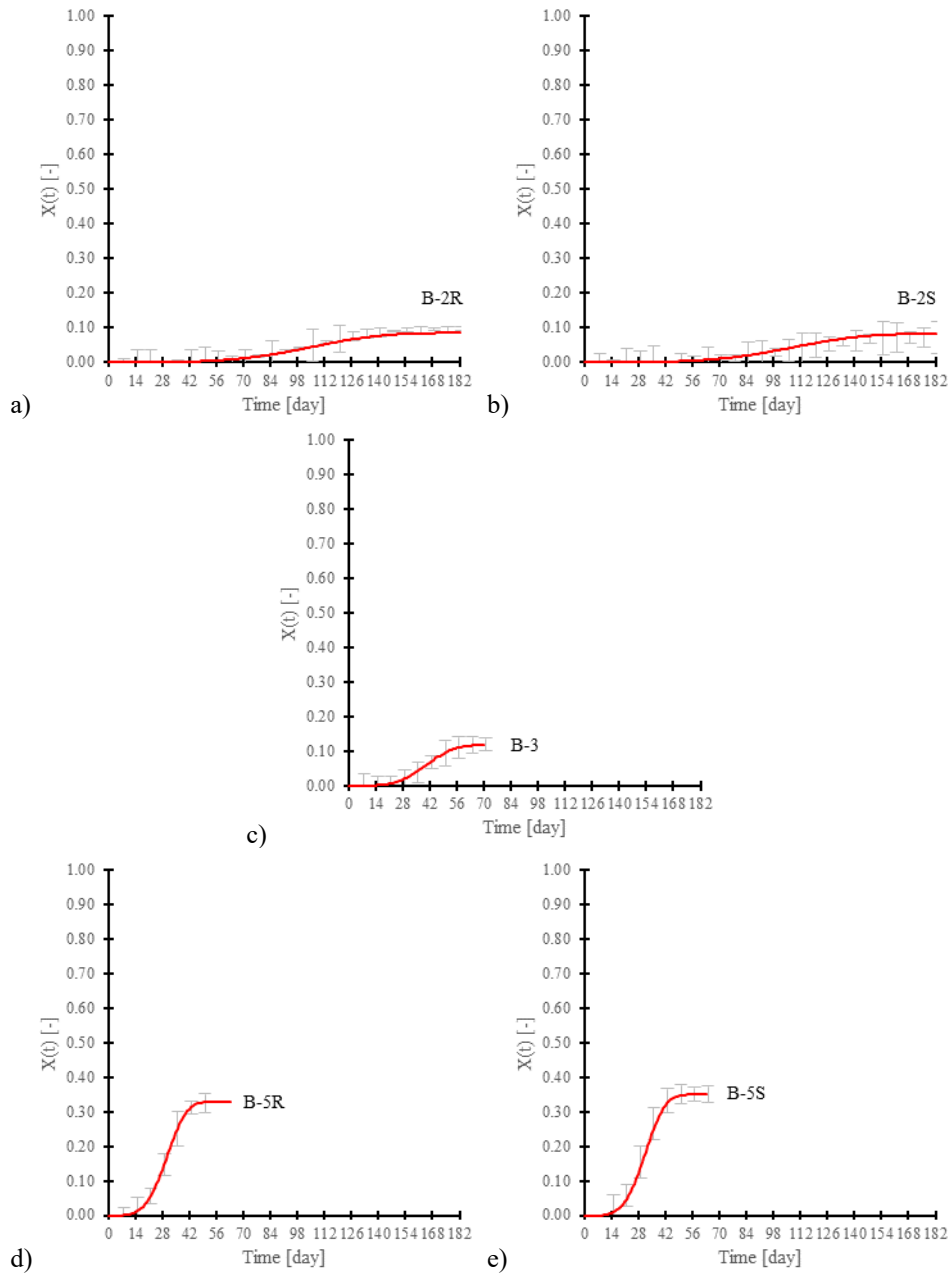


Figure 7.6. Growth curves, calculated with the implemented failure model, on the fired brick materials tested in this research under cold temperature (Test_5). Vertical lines indicate the standard errors of experimental measurements.

Figure 7.7 shows the growth curves obtained by the new failure model (7) calibrated for stones and the original experimental data found in literature [22]. At first sight, the failure model well overlapped the experimental values.

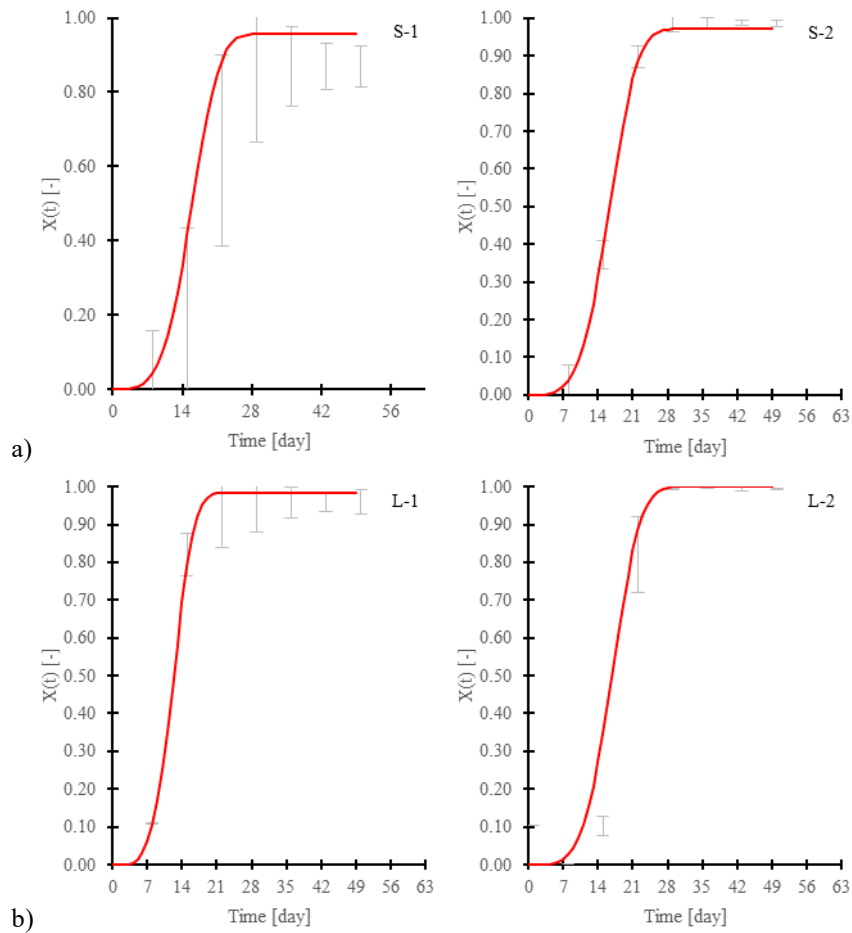


Figure 7.7. Growth curves, calculated with the implemented failure model, on the stone materials: a) sandstones and b) limestones; tested under optimal environmental conditions (Test_0). Vertical line bars indicate experimental standard deviations.

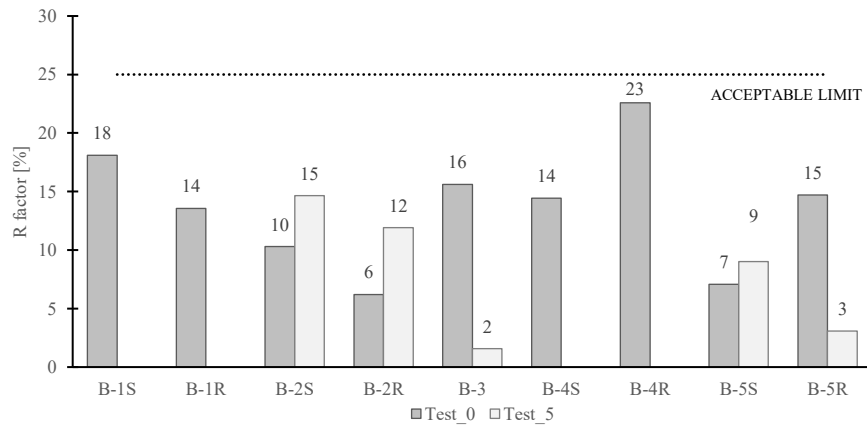
On this type of material, at the end of the biofouling process (almost 49 days), the algal coverage could reach up to 100% of the samples' surface.

It should be remembered that the stone substrates were characterized by considerable lower values of porosity, roughness and total pore area, if compared to the tested fired bricks. Despite this difference the corrective coefficient determined for stones (see Section 7.5) were confirmed to be adequate to simulate the real biofouling measured on stone substrates.

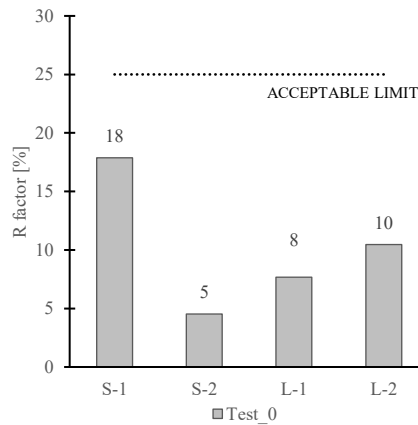
The analytical validation of the failure model was performed by determining the confidential R factor (Figure 7.8) for each material, calculated according to equation (13), representing the gap between the experimental curve and the analytical curve.

Regarding the fired bricks (Figure 7.8a), under optimal growth conditions (Test_0) all the tested samples showed R factors comprised between 6% and 23%, while for $T = 10 \pm 2.5$ °C (Test_5) R factors were lower than 15%.

In Figure 7.8b the confidential R factors for the limestone and sandstone samples are reported. All the values were very low, with the maximum equal to 18% (material S-1).



a)



b)

Figure 7.8. R factor values for a) fired brick materials and b) stone materials. Dotted lines indicate the limit of an acceptable R factor.

Finally, to validate the results, the R factors of this study were compared to the R factors calculated in other researches on similar building materials. The acceptable limit (25%) reported in Figure 7.8 was set according to the R factors reported in literature [19–21]. The R factors obtained in this work were always lower than the acceptable limit.

In conclusion, for all the investigated materials a good agreement between the simulated biofouling and the experimental data was obtained. Hence, it can be assessed that the failure model well simulated the algal biofouling both on fired brick and stone surfaces under different environmental conditions.

Chapter 8

Conclusions

Previous studies showed that the modified Avrami's model is able to well simulate algal growth on building materials under optimal environmental conditions. However, a failure model able to predict algae growth on building materials, explicitly considering the influence of variable environmental conditions, as well as the substrate properties, on the algae growth has not been developed yet. This work tried to fill this gap considering the parameters that mostly influence the algal growth: the total porosity, roughness and total pore area of the substrate, as well as and temperature and relative humidity among the environmental conditions.

Up to now, researches, with particular reference to fired bricks, have shown the important role of the substrate in biofouling. However, all these studies referred to tests usually performed under optimal conditions of temperature and relative humidity, without considering the influence of non-constant environmental conditions, whose role was instead taken into account in this research. In this work, the effects of the environmental conditions were assessed carrying out accelerated growth test of *Chlorella mirabilis* and *Chroococcidiopsis fissurarum* stains, with water "run-off cycles" apparatus, on building materials exposed to different relative humidities and temperatures.

Concerning the investigations about the effect of relative humidity, the colorimetric variations detected on samples' surfaces exposed to $RH \leq 98\%$ were lower than the perceptible threshold for human eye. Quantitative analysis (DIA) confirmed this result, since no covered area by algae was detected onto any samples' surface at the tested RHs. Thus, experimental findings showed that there was no growth at the tested relative humidities, and, from an engineering standpoint, $RH < 98\%$ could be considered as a safety limit against algae growth. Therefore, it can be reasonably assumed that the phenomenon of growth can only occur in presence of free water on the material surface.

According to the accelerated growth tests carried out under different temperatures, it was found that algal biofouling was highly influenced by the temperature conditions. The colder temperature reduced the rate of the biofouling process and the covered area at the end of the tests significantly decreased, if compared to the exposure under optimal temperature.

Thanks to the experimental results, it was confirmed the role of the substrate on algae growth: high porosity and high roughness influenced the colonization in terms of time and covered area at the end of the process. Indeed, the lower the porosity the higher is the stagnation time, since the microorganisms need time to join from a pore to another one. Moreover, the higher the roughness the higher is the covered area, because the micro-asperities of the substrate favour the mechanical anchorage of the microorganisms.

Experimental results were then analytically analysed, and it was confirmed that the previous modified Avrami's model was able to predict algae growth, not only for optimal temperature conditions, but also for colder ones. Subsequently the previous Avrami's model was implemented, by introducing variables related to the substrate properties (total porosity,

roughness and total pore area) and to the environmental conditions (temperature and relative humidity).

Results demonstrated that the new failure model is still suitable to describe the algal biofouling over the time, for different material substrates (fired brick and stones) and also to predict the overall process of covered area under non-optimal environmental conditions.

Moreover, from an engineering standpoint, this failure model can be considered a promising tool. By implementing the obtained mathematical equations into a hygrothermal calculation software, it could be possible to determine the biofouling process on different building façades. In addition, this new tool would help in the prediction of the service life of a certain structural design in critical temperature and humidity conditions, supporting the engineers in developing and/or providing guidelines for interventions and maintenance techniques.

This study was based on brick and stone material data, but other different materials and different environmental conditions should be investigated to extend the feasibility of the model (by determining the new material corrective coefficients and by validating the scale functions regarding environmental conditions), as well as different algae strains should be tested to consider the various colonizers of the façades. In addition, the model was based only on data experimentally collected under controlled conditions. Field-scale results should be performed and compared to laboratory data to enhance the predictive capability of the model to uncontrolled conditions.

References

- [1] RIBuild - Robust Internal Thermal Insulation of Historic Buildings. CAll: H2020-EE-2014-2015/H2020-EE-2014-1-PPP. Grant Agreement number: 637268.
- [2] H. M. Künzeli, "Effect of interior and exterior insulation on the hygrothermal behaviour of exposed walls," *Mater. Struct.*, vol. 31, no. 2, pp. 99–103, 1998.
- [3] G. Scheffler and J. Grunewald, "Material development and optimisation supported by numerical simulation for a capillary-active inside insulation material," *Res. Build. Phys.*, pp. 77–85, 2003.
- [4] K. Ueno and J. Strauße, "Field monitoring and simulation of a historic mass masonry building," *Proc. Build. XII*, no. December 2013, pp. 1–16, 2013.
- [5] T. De Mets, A. Tilmans, and X. Loncour, "Hygrothermal assessment of internal insulation systems of brick walls through numerical simulation and full-scale laboratory testing," *Energy Procedia*, vol. 132, pp. 753–758, 2017.
- [6] M. Morelli and S. Svendsen, "Investigation of interior post-insulated masonry walls with wooden beam ends," *J. Build. Phys.*, vol. 36, no. 3, pp. 265–273, 2013.
- [7] M. Morelli, T. R. Nielsen, G. A. Scheffler, and S. Svendsen, "Internal Insulation of Masonry Walls with Wooden Floor Beams in Northern Humid Climate," *Therm. Perform. Exter. Envel. Whole Build. XI Int. Conf.*, no. 2009, 2010.
- [8] M. Harrestrup and S. Svendsen, "Full-scale test of an old heritage multi-storey building undergoing energy retrofitting with focus on internal insulation and moisture," *Build. Environ.*, vol. 85, pp. 123–133, Feb. 2015.
- [9] J. Straube, C. Schumacher, and P. Mensinga, "Assessing the Freeze- Thaw Resistance of Clay Brick for Interior Insulation Retrofit Projects," *Therm. Perform. Exter. Envel. Whole Build. XI Int. Conf.*, 2010.
- [10] A. Holm, W. Zillig, and H. M. Künzeli, "Exterior Surface Temperature and Humidity of Walls - Comparison of Experiment and Numerical Simulation," in *Proceedings of Performance of Exterior Envelopes of Whole Buildings IX*, 2004.
- [11] E. Vereecken and S. Roels, "Review of mould prediction models and their influence on mould risk evaluation," *Build. Environ.*, vol. 51, pp. 296–310, 2012.
- [12] K. Sedlbauer, "Prediction of mould fungus formation on the surface of and inside building components," 2001.
- [13] A. Hukka and H. Viitanen, "A mathematical model of mould growth on wooden material," *Wood Sci. Technol.*, vol. 33, pp. 475–485, 1999.

- [14] T. Ojanen, H. Viitanen, R. Peuhkuri, K. Lähdesmäki, J. Vinha, and K. Salminen, "Mold Growth Modeling of Building Structures Using Sensitivity Classes of Materials," *Therm. Perform. Exter. Envel. Build. XI*, pp. 1–10, 2010.
- [15] J. A. Clarke *et al.*, "A technique for the prediction of the conditions leading to mould growth in buildings," *Build. Environ.*, vol. 34, no. 4, pp. 515–521, Jul. 1999.
- [16] International Energy Agency, "Guidelines and Practice," *Annex XIV Condens. Energy*, 1990.
- [17] E. Vereecken, D. Saelens, and S. Roels, "A comparison of different mould prediction models," *Proc. Build. Simul. 2011 12th Conf. Int. Build. Perform. Simul. Assoc.*, vol. 6, no. M, pp. 1934–1941, 2011.
- [18] B. Ruot and H. Barberousse, "Quantification and Kinetic Modeling of the Colonisation of Façades Rendering Mortar by Algae," *Vii Sbta*, pp. 1–12, 2007.
- [19] T. H. Tran *et al.*, "Avrami's law based kinetic modeling of colonization of mortar surface by alga *Klebsormidium flaccidum*," *Int. Biodeterior. Biodegrad.*, vol. 79, pp. 73–80, 2013.
- [20] L. Graziani, E. Quagliarini, and M. D'Orazio, "The role of roughness and porosity on the self-cleaning and anti-biofouling efficiency of TiO₂-Cu and TiO₂-Ag nanocoatings applied on fired bricks," *Constr. Build. Mater.*, vol. 129, pp. 116–124, 2016.
- [21] L. Graziani, E. Quagliarini, and M. D'Orazio, "TiO₂-treated different fired brick surfaces for biofouling prevention: Experimental and modelling results," *Ceram. Int.*, vol. 42, no. 3, pp. 4002–4010, 2016.
- [22] L. Graziani and E. Quagliarini, "On the Modelling of Algal Biofouling Growth on Nano-TiO₂ Coated and Uncoated Limestones and Sandstones," *Coatings*, vol. 8, no. 2, p. 54, 2018.
- [23] T. Verdier, M. Coutand, A. Bertron, and C. Roques, "A review of indoor microbial growth across building materials and sampling and analysis methods," *Build. Environ.*, vol. 80, pp. 136–149, Oct. 2014.
- [24] K. Gradeci, N. Labonnote, B. Time, and J. Köhler, "A probabilistic-based methodology for predicting mould growth in façade constructions," *Build. Environ.*, vol. 128, pp. 33–45, Jan. 2018.
- [25] Q. Wang and T. Zhang, "Review of mathematical models for biofilms," *Solid State Commun.*, vol. 150, no. 21–22, pp. 1009–1022, Jun. 2010.
- [26] P. Steskens, X. Loncour, S. Roels, and E. Vereecken, "Interior Insulation of masonry walls – An assessment method," in *Internationaler Innendämmkongress*, no. September, pp. 62–69, 2013.

- [27] J. Straube and C. Schumacher, "Interior Insulation Retrofits of Load-Bearing Masonry Walls in Cold Climates," *J. Green Build.*, vol. 2, no. 2, pp. 42–50, 2007.
- [28] E. Vereecken and S. Roels, "A comparison of the hygric performance of interior insulation systems: A hot box-cold box experiment," *Energy Build.*, vol. 80, pp. 37–44, 2014.
- [29] A. Abdul Hamid and P. Wallentén, "Hygrothermal assessment of internally added thermal insulation on external brick walls in Swedish multifamily buildings," *Build. Environ.*, vol. 123, pp. 351–362, 2017.
- [30] M. Saïd and Pe. R. Demers LL McSheffrey, "Hygrothermal performance of a masonry wall retrofitted with interior insulation," *Res. Build. Phys.*, pp. 445–454, 2003.
- [31] E. Vereecken and S. Roels, "Capillary active interior insulation: do the advantages really offset potential disadvantages?," *Mater. Struct. Constr.*, vol. 48, no. 9, pp. 3009–3021, 2015.
- [32] T. Odgaard, S. P. Bjarløv, and C. Rode, "Interior insulation – Experimental investigation of hygrothermal conditions and damage evaluation of solid masonry façades in a listed building," *Build. Environ.*, vol. 129, pp. 1–14, Feb. 2018.
- [33] E. Biseniece *et al.*, "Thermal performance of internally insulated historic brick building in cold climate: A long term case study," *Energy Build.*, vol. 152, pp. 577–586, 2017.
- [34] J. F. Straube, K. Ueno, and C. J. Schumacher, "Measure Guideline: Internal Insulation of Masonry Walls," Golden, CO (United States), Jul. 2012.
- [35] E. Vereecken, L. Van Gelder, H. Janssen, and S. Roels, "Interior insulation for wall retrofitting - A probabilistic analysis of energy savings and hygrothermal risks," *Energy Build.*, vol. 89, pp. 231–244, 2015.
- [36] H. M. Künzle, "Factors determining surface moisture on external walls," *Build. X*, p. 6, 2007.
- [37] M. Uranjek and V. Bokan-Bosiljkov, "Influence of freeze–thaw cycles on mechanical properties of historical brick masonry," *Constr. Build. Mater.*, vol. 84, pp. 416–428, 2015.
- [38] S. Bjarløv, G. Finken, and T. Odgaard, "Retrofit with Interior Insulation on Solid Masonry Walls in Cool Temperate Climates – An Evaluation of the influence of Interior Insulation Materials on Moisture Condition in the Building Envelope," *Energy Procedia*, vol. 78, pp. 1461–1466, 2015.
- [39] J. Zhao, J. Grunewald, U. Ruisinger, and S. Feng, "Evaluation of capillary-active mineral insulation systems for interior retrofit solution," *Build. Environ.*, vol. 115, pp. 215–227, 2017.

- [40] G. R. Finken, S. P. Bjarløv, and R. H. Peuhkuri, "Effect of façade impregnation on feasibility of capillary active thermal internal insulation for a historic dormitory – A hygrothermal simulation study," *Constr. Build. Mater.*, vol. 113, 2016.
- [41] J. Toman, A. Vimmrová, and R. Černý, "Long-term on-site assessment of hygrothermal performance of interior thermal insulation system without water vapour barrier," *Energy Build.*, vol. 41, pp. 51–55, 2009.
- [42] S. Johansson, "Biological growth on mineral façades," 2005.
- [43] H. Venzmer, J. Von Werder, N. Lesnych, and L. Koss, "Algal defacement of facade materials - results of a long term natural weathering tests obtained by new diagnostic tools," *Proc. 8th Symp. Build. Phys. Nord. Ctries.*, vol. 1, pp. 277–284, 2008.
- [44] C. A. Crispim, P. M. Gaylarde, and C. C. Gaylarde, "Algal and cyanobacterial biofilms on calcareous historic buildings," *Curr. Microbiol.*, vol. 46, no. 2, pp. 79–82, 2003.
- [45] P. Tiano, "Biodegradation of Cultural Heritage: Decay Mechanisms and Control Methods," *CNR-Centro di Stud. Sulle Cause Deperimento e Metod. Conserv. Opere d'Arte*, vol. 9, pp. 1–37, 2001.
- [46] C. Saiz-Jimenez, "Biodeterioration of stone in historic buildings and monuments," *Biodeterior. Res.* 4, pp. 587–604, 1994.
- [47] C. Gaylarde, M. Ribas Silva, and T. Warscheid, "Microbial impact on building materials: an overview," *Mater. Struct.*, vol. 36, no. 5, pp. 342–352, 2003.
- [48] A. Z. Miller *et al.*, "Bioreceptivity of building stones: A review," *Sci. Total Environ.*, vol. 426, pp. 1–12, 2012.
- [49] R. Kumar and A. V. Kumar, *Biodeterioration of Stone in Tropical Environments*, vol. 20. 1999.
- [50] I. Flores-Colen, J. de Brito, and V. P. de Freitas, "Stains in facades' rendering - Diagnosis and maintenance techniques' classification," *Constr. Build. Mater.*, vol. 22, no. 3, pp. 211–221, 2008.
- [51] H. Barberousse, R. J. Lombardo, G. Tell, and A. Couté, "Factors involved in the colonisation of building façades by algae and cyanobacteria in France," *Biofouling*, vol. 22, no. 2, pp. 69–77, 2006.
- [52] P. Lopez-Arce and J. Garcia-Guinea, "Weathering traces in ancient bricks from historic buildings," *Build. Environ.*, vol. 40, no. 7, pp. 929–941, 2005.
- [53] L. Hoffmann, *Algae of terrestrial habitats*, vol. 55, no. 2. 1989.
- [54] B. Amaro, D. Saraiva, J. De Brito, and I. Flores-Colen, "Inspection and diagnosis system of ETICS on walls," *Constr. Build. Mater.*, vol. 47, no. October, pp. 1257–1267, 2013.

- [55] L. G. V. Verhoef, "Soiling and cleaning of building facades," London: Chapman and Hall, 1988.
- [56] C. C. Gaylarde and P. M. Gaylarde, "A comparative study of the major microbial biomass of biofilms on exteriors of buildings in Europe and Latin America," *Int. Biodeterior. Biodegrad.*, vol. 55, no. 2, pp. 131–139, 2005.
- [57] C. Adam, "Algen, Schimmel und Flechten. 1. teil," *Das Dtsch. Malerblatt* 61(3) 28-30, 1990.
- [58] W. Hofbauer, K. Breuer, and K. Sedlbauer, "Algen, Flechten, Moose und Farne auf Fassaden," *Aufsatz*, vol. 25, no. November, pp. 383–396, 2003.
- [59] H. K. Kastien, "Algen und Pilze an mineralischen Fassaden," vol. 10–11, pp. 57–62, 1999.
- [60] B. Pattanaik and S. P. Adhikary, "Blue-green algal flora at some archaeological sites and monuments of India," *Feddes Repert.*, vol. 113, no. 3–4, pp. 289–300, Aug. 2002.
- [61] E. Imre Friedmann and R. Ocampo-Friedmann, "A primitive cyanobacterium as pioneer microorganism for terraforming Mars," *Advances in Space Research*, vol. 15, no. 3, pp. 243–246, 1995.
- [62] D. Billi, "Genetic tools for desiccation- and radiation-tolerant cyanobacteria of the genus *Chroococcidiopsis*," *Gene*, pp. 1517–1521, 2010.
- [63] J. J. Ortega-Calvo, X. Ariño, M. Hernandez-Marine, and C. Saiz-Jimenez, "Factors affecting the weathering and colonization of monuments by phototrophic microorganisms," *Sci. Total Environ.*, vol. 167, no. 1–3, pp. 329–341, 1995.
- [64] W. Zillig, K. Lenz, K. Sedlbauer, and M. Krus, "Condensation on façades - influences of construction type and orientation," *Res. Build. Phys.*, pp. 437–444, 2003.
- [65] D. Giovannacci *et al.*, "Algal colonization kinetics on roofing and façade tiles: Influence of physical parameters," *Constr. Build. Mater.*, vol. 48, pp. 670–676, 2013.
- [66] T. H. Tran *et al.*, "Influence of the intrinsic characteristics of mortars on biofouling by *Klebsormidium flaccidum*," *Int. Biodeterior. Biodegradation*, vol. 70, pp. 31–39, May 2012.
- [67] T. H. Tran *et al.*, "Influence of the intrinsic characteristics of mortars on their biofouling by pigmented organisms: Comparison between laboratory and field-scale experiments," *Int. Biodeterior. Biodegrad.*, vol. 86, pp. 334–342, 2014.
- [68] L. Graziani, E. Quagliarini, and M. D'Orazio, "Application of titanium dioxide on clay brick façades for algal growth prevention," *Int. Mason. Conf. 2014*, no. 637268, pp. 1–9, 2014.

- [69] L. Graziani, E. Quagliarini, A. Osimani, L. Aquilanti, F. Clementi, and M. D’Orazio, “The influence of clay brick substratum on the inhibitory efficiency of TiO₂ nanocoating against biofouling,” *Build. Environ.*, vol. 82, pp. 128–134, 2014.
- [70] M. D’Orazio *et al.*, “Effects of water absorption and surface roughness on the bioreceptivity of ETICS compared to clay bricks,” *Build. Environ.*, vol. 77, pp. 20–28, 2014.
- [71] S. P. Singh and P. Singh, “Effect of temperature and light on the growth of algae species: A review,” *Renew. Sustain. Energy Rev.*, vol. 50, pp. 431–444, 2015.
- [72] M. Ota, M. Takenaka, Y. Sato, R. Lee Smith, and H. Inomata, “Effects of light intensity and temperature on photoautotrophic growth of a green microalga, *Chlorococcum littorale*,” *Biotechnol. Reports*, vol. 7, pp. 24–29, 2015.
- [73] A. Konopka and T. D. Brock, “Effect of temperature on blue-green algae (Cyanobacteria) in Lake Mendota,” *Appl. Environ. Microbiol.*, vol. 36, no. 4, pp. 572–576, 1978.
- [74] R. Serra-Maia, O. Bernard, A. Gonçalves, S. Bensalem, and F. Lopes, “Influence of temperature on *Chlorella vulgaris* growth and mortality rates in a photobioreactor,” *Algal Res.*, vol. 18, pp. 352–359, 2016.
- [75] K. Lengsfeld and M. Krus, “Microorganism on façades – reasons, consequences and measures,” pp. 0–7, 2001.
- [76] J. A. Raven and R. J. Geider, “Temperature and algal growth,” *New Phytol.*, vol. 110, no. 4, pp. 441–461, 1988.
- [77] S. P. Shukla, J. Kvíderová, J. Tříška, and J. Elster, “*Chlorella mirabilis* as a potential species for biomass production in low-temperature environment,” *Front. Microbiol.*, vol. 4, no. APR, pp. 1–12, 2013.
- [78] A. Z. Miller, A. Dionísio, L. Laiz, M. F. MacEdo, and C. Saiz-Jimenez, “The influence of inherent properties of building limestones on their bioreceptivity to phototrophic microorganisms,” *Ann. Microbiol.*, vol. 59, no. 4, pp. 705–713, 2009.
- [79] E. Di Giuseppe, *Nearly Zero Energy Buildings and proliferation of microorganisms*. Springer Netherlands, 2013.
- [80] B. Chen-Charpentier, “Numerical simulation of biofilm growth in porous media,” *J. Comput. Appl. Math.*, vol. 103, no. 1, pp. 55–66, Mar. 1999.
- [81] F. Clarelli, C. D. I. Russo, R. Natalini, and M. Ribot, “Mathematical models for biofilms on the surface of monuments,” *Appl. Ind. Math. Italy III, 9th Conf. SIMAI*, vol. 82, pp. 1–12, 2009.
- [82] F. Clarelli, C. Di Russo, R. Natalini, and M. Ribot, “A fluid dynamics model of the growth of phototrophic biofilms,” *J. Math. Biol.*, vol. 66, no. 7, pp. 1387–1408, 2013.

- [83] F. Clarelli, C. Di Russo, R. Natalini, and rib, “A fluid dynamics multidimensional model of biofilm growth: stability, influence of environment and sensitivity,” *Math. Med. Biol.*, pp. 1–26, 2015.
- [84] Melvin Avrami, “Kinetics of phase change. I: General Theory,” *J. Chem. Phys.*, vol. 7, pp. 1103–1112, 1939.
- [85] M. Avrami, “Kinetics of Phase Change. II Transformation-Time Relations for Random Distribution of Nuclei,” *J. Chem. Phys.*, vol. 8, no. 2, pp. 212–224, 1940.
- [86] M. Avrami, “Granulation, Phase Change, and Microstructure Kinetics of Phase Change. III,” *J. Chem. Phys.*, vol. 9, no. 2, pp. 177–184, 1941.
- [87] W. A. Johnson and R. F. Mehl, “Reaction kinetics in processes of nucleation and growth,” *Tranz AIME*, vol. 135, p. 416, 1939.
- [88] A. Khawam and D. R. Flanagan, “Solid-state kinetic models: Basics and mathematical fundamentals,” *J. Phys. Chem. B*, vol. 110, no. 35, pp. 17315–17328, 2006.
- [89] M. Fanfoni and M. Tomellini, “The Johnson-Mehl- Avrami-Kohnogorov model: A brief review,” *Nuovo Cim. D*, vol. 20, no. 7–8, pp. 1171–1182, 1998.
- [90] J. N. Hay, “Application of the modified avrami equations to polymer crystallisation kinetics,” *Br. Polym. J.*, vol. 3, no. 2, pp. 74–82, 1971.
- [91] M. Slováček, “Application of numerical simulation of heat treatment in industry,” *J. Phys. IV Fr.*, vol. 120, pp. 753–760, 2004.
- [92] A. K. Jena and M. C. Chaturvedi, *Phase transformation in materials*. Englewood Cliffs, N.J: Prentice Hall, 1992.
- [93] F. Gladis and R. Schumann, “Influence of material properties and photocatalysis on phototrophic growth in multi-year roof weathering,” *Int. Biodeterior. Biodegradation*, vol. 65, no. 1, pp. 36–44, Jan. 2011.
- [94] O. Guillitte and R. Dreesen, “Laboratory chamber studies and petrographical analysis as bioreceptivity assessment tools of building materials,” *Sci. Total Environ.*, vol. 167, no. 1–3, pp. 365–374, 1995.
- [95] E. Quagliarini *et al.*, “Effect of temperature and relative humidity on algae biofouling on different fired brick surfaces,” *Constr. Build. Mater.*, vol. 199, pp. 396–405, 2019.
- [96] O. Guillitte, “Bioreceptivity: a new concept for building ecology studies,” *Sci. Total Environ.*, vol. 167, no. 1–3, pp. 215–220, 1995.
- [97] H. Barberousse, “Etude de la diversité des algues et des cyanobactéries colonisant les revêtements de façade en France et recherche des facteurs favorisant leur implantation,” 2007.

- [98] A. Dubosc, "Etude de developement de salissures biologiques sur les parements en beton: mise au point d'essais acceleres de vieillissement," *Lab. Matériaux Durabilité des Constr.*, 2000.
- [99] J. Radulovic *et al.*, "Biofouling resistance and practical constraints of titanium dioxide nanoparticulate silane/siloxane exterior facade treatments," *Build. Environ.*, vol. 68, pp. 150–158, 2013.
- [100] H. Barberousse, B. Ruot, C. Yéprémian, and G. Boulon, "An assessment of façade coatings against colonisation by aerial algae and cyanobacteria," *Build. Environ.*, vol. 42, no. 7, pp. 2555–2561, 2007.
- [101] G. Escadeillas, A. Bertron, E. Ringot, P. J. Blanc, and A. Dubosc, "Accelerated testing of biological stain growth on external concrete walls. Part 2: Quantification of growths," *Mater. Struct.*, vol. 42, no. 7, pp. 937–945, 2009.
- [102] T. Martinez, A. Bertron, G. Escadeillas, and E. Ringot, "Algal growth inhibition on cement mortar: Efficiency of water repellent and photocatalytic treatments under UV/VIS illumination," *Int. Biodeterior. Biodegrad.*, vol. 89, pp. 1150–125, 2014.
- [103] A. Dubosc, G. Escadeillas, and P. J. Blanc, "Characterization of biological stains on external concrete walls and influence of concrete as underlying material," *Cem. Concr. Res.*, vol. 31, no. 11, pp. 1613–1617, 2001.
- [104] W. De Muynck, A. M. Ramirez, N. De Belie, and W. Verstraete, "Evaluation of strategies to prevent algal fouling on white architectural and cellular concrete," *Int. Biodeterior. Biodegrad.*, vol. 63, no. 6, pp. 679–689, 2009.
- [105] L. Graziani *et al.*, "Evaluation of inhibitory effect of TiO₂ nanocoatings against microalgal growth on clay brick façades under weak UV exposure conditions," *Build. Environ.*, vol. 64, pp. 38–45, 2013.
- [106] L. Graziani and M. D'Orazio, "Biofouling Prevention of Ancient Brick Surfaces by TiO₂-Based Nano-Coatings," *Coatings*, vol. 5, no. 3, pp. 357–365, 2015.
- [107] E. Quagliarini, L. Graziani, D. Diso, A. Licciulli, and M. D'Orazio, "Is nano-TiO₂ alone an effective strategy for the maintenance of stones in Cultural Heritage?," *J. Cult. Herit.*, vol. 30, pp. 81–91, 2018.
- [108] F. Stazi, B. Gregorini, A. Gianangeli, G. Bernardini, and E. Quagliarini, "Design of a smart system for indoor climate control in historic underground built environment," *Energy Procedia*, vol. 134, pp. 518–527, 2017.
- [109] B. Gregorini, G. Bernardini, A. Gianangeli, E. Quagliarini, and M. D'Orazio, "A 'smart' low-impact system for guaranteeing sustainable visitors' access," in *6th International Conference on Heritage and Sustainable Development*, 2018.

- [110] B. Gregorini, G. Bernardini, A. Gianangeli, E. Quagliarini, and M. D’Orazio, “Building Heritage Cognitivo: un sistema per la gestione e la conservazione dell’edificio storico,” in *Colloqui.AT.e 2018. Edilizia Circolare*, 2018.
- [111] B. Gregorini, A. Gianangeli, G. Bernardini, M. D’Orazio, and E. Quagliarini, “La conservazione dell’ambiente ipogeo di Palazzo Campana: monitoraggi e prove di caratterizzazione propedeutici all’intervento,” in *6th International Conference, ReUSO*, 2018.
- [112] A. Gianangeli, E. Di Giuseppe, and M. D’Orazio, “Mould growth risk evaluation of internal insulation solutions in a historic building under temperate climates,” in *SER4SC 2018 Seismic and Energy Renovation for Sustainable Cities - Conference Proceedings*, 2018, pp. 508–517.
- [113] L. Tomaselli, G. Lamenti, M. Bosco, and P. Tiano, “Biodiversity of photosynthetic micro-organisms dwelling on stone monuments,” *Int. Biodeterior. Biodegrad.*, vol. 46, no. 3, pp. 251–258, 2000.
- [114] I. Lupan and O. Popescu, “Metagenomics and future perspectives for biodeterioration and biodegradation studies,” *Ann. Rom. Soc. Cell Biol.*, vol. 17, no. 2, pp. 37–42, 2012.
- [115] ASTM D5589-09. Standard test method for determining the resistance of paint films and related coatings to algal defacement.
- [116] R. Giuseppe, *Istituzioni di restauro dei beni architettonici e ambientali*. 1990.
- [117] C. F. Giuliani, *L’edilizia nell’antichità*. 1993.
- [118] ASTM D4404-10. Standard test method for determination of pore volume and pore volume distribution of soil and rock by mercury intrusion porosimetry.
- [119] UNI EN ISO 4287:2009. Geometrical Product Specifications (GPS) – Surface texture: Profile Method – Terms, Definitions and Surface Texture Parameters.
- [120] J. C. Gwo, J. Y. Chiu, C. C. Chou, and H. Y. Cheng, “Cryopreservation of a marine microalga, *Nannochloropsis oculata* (Eustigmatophyceae),” *Cryobiology*, vol. 50, no. 3, pp. 338–343, 2005.
- [121] UNI EN ISO 12571:2013. Hygrothermal performance of building materials and products - Determination of hygroscopic sorption properties.
- [122] *Chemical Engineers’ Handbook. Second edition (Perry, John H., ed.)*, vol. 19, no. 9. 1942.
- [123] G. Escadeillas, A. Bertron, E. Ringot, P. J. Blanc, and A. Dubosc, “Accelerated testing of biological stain growth on external concrete walls. Part 1: Quantification of growths,” *Mater. Struct.*, vol. 42, no. 7, pp. 937–945, 2009.

- [124] UNI EN 15886:2010. Conservation of cultural property - Test methods - Colour measurement of surfaces.
- [125] UNI 11721:2018. Materiali lapidei - Metodi di prova – Misurazione preventiva della variazione colorimetrica di superfici di pietra.
- [126] E. Franzoni, A. Fregni, R. Gabrielli, G. Graziani, and E. Sassoni, “Compatibility of photocatalytic TiO₂-based finishing for renders in architectural restoration: A preliminary study,” *Build. Environ.*, vol. 80, pp. 125–135, 2014.
- [127] C. A. Schneider, W. S. Rasband, and K. W. Eliceiri, “NIH Image to ImageJ: 25 years of image analysis,” *Nat. Methods*, vol. 9, no. 7, pp. 671–675, 2012.
- [128] F. Tiago and R. Wayne, *The ImageJ User Guide*. 2011.
- [129] J. Gao, F. Gu, N. H. Abdella, H. Ruan, and G. He, “Investigation on Culturable Microflora in Tibetan Kefir Grains from Different Areas of China,” *J. Food Sci.*, vol. 77, no. 8, 2012.
- [130] C. Garofalo *et al.*, “Bacteria and yeast microbiota in milk kefir grains from different Italian regions,” *Food Microbiol.*, vol. 49, no. 1, pp. 123–133, 2015.
- [131] M. Ghouh and S. Mitri, “The Ecology and Evolution of Microbial Competition,” *Trends Microbiol.*, vol. 24, no. 10, pp. 833–845, 2016.
- [132] P. Häupl and H. Fechner, “Hygic Material Properties of Porous Building Materials,” *J. Build. Phys.*, vol. 26, no. 3, pp. 259–284, 2003.
- [133] M. Krus and K. Kiej, “Determination of the moisture storage characteristics of porous capillary active materials,” *Mater. Struct.*, vol. 31, no. October, pp. 522–529, 1998.